12-16-2015

Adaptive PI Control to Realize Sinusoidal Ripple Current Charging in Battery Charger Systems

Jen-Guey Chen
University of Connecticut, jen-guey.chen@uconn.edu

Adaptive PI Control to Realize Sinusoidal Ripple Current Charging in Battery Charger Systems

Jen-Guey Chen

B.E., Yuan-Ze University, 2012

A Thesis

Submitted in Partial Fulfillment of the

Requirements for the Degree of

Master of Science

At the

University of Connecticut

2015

APPROVAL PAGE

Masters of Science Thesis

Adaptive PI Control to Realize Sinusoidal Ripple Current Charging in Battery Charger Systems

Presented by

Jen-Guey Chen, B.E.

Major Advisor_____
Dr. Sung-Yeul Park

Associate Advisor_____
Dr. Yang Cao

Associate Advisor_____
Dr. Ali M. Bazzi

University of Connecticut

2015

ACKNOWLEDGEMENTS

Firstly, I would like to express my sincere gratitude to my advisor Prof. Sung-Yeul Park for the continuous support of my M.S study and related research, for his patience, motivation, and immense knowledge. His guidance helped me in all the time of research and writing of this thesis. Besides my advisor, I would like to thank the rest of my committee: Prof. Ali.M Bazzi, and Dr. Yang Cao, for their insightful comments and encouragement, but also for the hard question which guided me to straighten my research topic.

My sincere thanks also goes to Dr. Yong-Duk Lee, who taught me the procedure of how to do the research, how to manage my time and how to organize the problems as well as the idea. Without his precious support it would not be possible to conduct this research.

I thank my lab mates for their assistance in the lab, Joshua Ivaldi, Shawn Maxwell, S.M Rakiul Islam and M.D Kamal Hossain. I would like to express my thankfulness to all of them. Since I did have difficulties on learning new method or devices smoothly, they were willing to spend their time on me.

Last but not the least, I would like to thank my parents and my girlfriend for supporting me spiritually throughout writing this thesis and my life in general.

CONTENTS

LIST OF FIGURES

LIST OF TABLES

ABSTRACT

This thesis proposes the adaptive PI gain control to regulate sinusoidal ripple current (SRC) in battery charger systems. The SRC charge method is suited for fast and efficient charging. Y.D Lee (2015) propose that SRC charge method can reduce the charging time, decrease the charging temperature and improve the charging efficiency by applying optimal frequency to charge the battery. In order to determine optimal frequency for charging, the swept frequency is required in SRC charge method. Therefore, in order to perform SRC charge approach, the battery charger systems have to be capable of handling swept frequency input and regulating high frequency ripple current. However, the conventional designed charger would not be able to satisfy the aforementioned requirements because the control bandwidth of a fixed PI control gains is not designed for SRC but for a constant current profile. Therefore, the fixed PI gain control is limited to regulate the wide range frequency of ripple current. In this thesis, the limitations in the application of the SRC method to an existing battery charger is investigated and analyzed. The solution to the aforementioned issue is to apply the adaptive PI gain control based on Model Reference Adaptive Control (MRAC) so that it can regulate variable frequency of charging ripple current. The proposed approach shows that MRAC is the suitable solution for SRC charging because it is easily equipped into the conventional PI controller of a digital signal processor without any adjustments to the hardware design. As a result, there is no attenuation and phase delay under variable ripple frequencies condition (1~600 Hz). The performance of current control is compared with conventional fixed PI gain and the proposed adaptive variable gain. The

proposed method is verified with simulation and experimental results.

I. INTRODUCTION

1.1 Overview of battery charger systems

A battery charger is a device applied to provide energy to rechargeable battery or secondary battery by forcing current through it. In the battery-powered equipment, such as cell phone, digital camera and laptop, the power adapter may be described as chargers. Technically, the battery charger refers to the internal regulator, such as linear regulator or dc-dc converter. The purpose of the battery charger is not only to provide a voltage and current to the battery but also to prevent the battery from overcharging and overheating. The typical battery charger consists of a dc-dc converter that provides the regulated and filtered voltage and current and a controller that determines the charging method. Rechargeable batteries are important to both portable electronic equipment and higher power level equipment such as electric vehicles (EVs) and battery energy and storage system (BESS). The charging circuits must be carefully designed and highly dependent on the particular specifications and the battery's chemistry. The most popular types of rechargeable batteries in use today are the Sealed-Lead-Acid, Nickel-Cadmium (NiCd), Nickel-Metal-Hydride (NiMH), and Lithium-Ion (Li-Ion). Among them, Li-Ion batteries are already considered the preferred option for many portable applications because it offers a high capacity-to-size (weight) ratio and a low self-discharge characteristic [1]. There are many considerations and trade-offs needed to be taken into account when designing the appropriate charging circuits. Weight, capacity, and cost are the primary considerations in most portable electronic equipment [2]. However, these considerations are not only relating but often conflicting. For example, slow charging circuits are relatively simple and cheap, while fast

charging circuits are more complex and are required to prevent the battery from overcharging and overheating. For this reason, fast charging circuits typically have a built-in protection approach, such as battery management system (BMS) to protect the battery during the charging operation. The following subsection introduces different battery charger applications based on different power levels.

1.2 Battery charger applications

1.2.1 Cell phone battery charger system

A. Introduction

Cell phones have become an ubiquitous device in our life. The increasing penetration of cell phones is a phenomenon experienced worldwide during the past years. As a consequence, there has been a proliferation of small wall plug-in ac-dc adapters required for charging the batteries (NiCd, NiMH, or Li-ion) of the cell phone. Li-ion technology is currently the best battery candidate among the battery technology for small portable devices due to its high energy density, low self-discharge characteristics, and tremendous flexibility in size and shape [3].

B. System configuration

There are two options for the power-management circuit designers to choose from in the configuration for the cell phone power battery system. They can either isolate the battery from the load while charging the battery, powering the load directly from the adapter, as shown in Fig.1.1. Or they can connect the battery and the load in series, powering the load with the battery while charging the battery from the adapter, as shown in Fig.1.2.

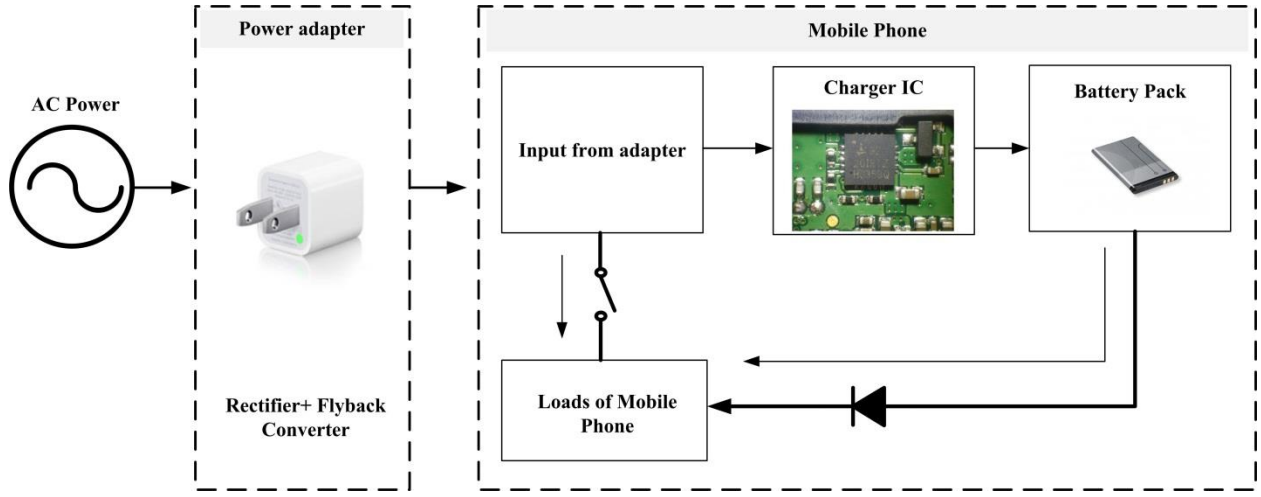

Fig.1.1. Cell-phone power system configuration: isolation from the load to the battery

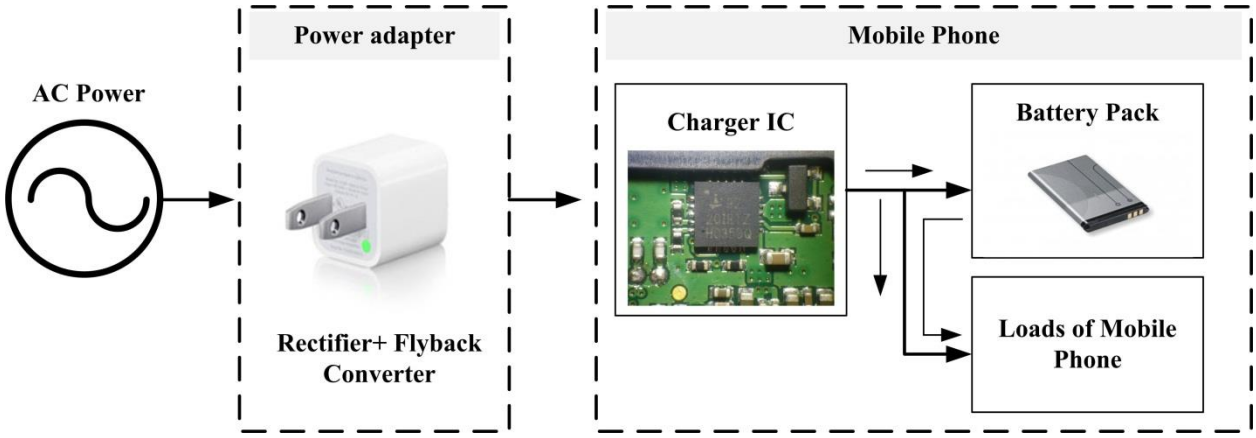

Fig.1.2. Cell-phone power system configuration: direct connection of the battery to the load.

There are many commercial battery charger ICs that apply either isolation or direct connection. Both of the connection topologies have their own advantages and disadvantages. In the market perspective, simple, compact and low-cost are the major concerns of the battery charger; therefore, the direct connection topology is getting more popular and attractive to be implemented in the battery charger ICs [4]. Table I summarizes the advantages and disadvantages of each configuration:

TABLE I. [4]

THE COMPARISON BETWEEN ISOLATION AND DIRECT CONNECTION CONFIGURATION

	Advantages	Disadvantages
Isolation topology	1. Enable the load to be operated under pre-charge threshold voltage. 2. Carry high system load current.	1. More counts of components. 2. The regulator of the load has to tolerate input transients and noises from the adapter.
Direct connection topology	1. Simple design, compact and low-cost. 2. Continuity of load power. 3. The input power to the load is well-regulated by the regulator. 4. Reduce the supply-voltage transients.	1. Unable to power the load that is below pre-charge threshold voltage.

There are several topologies that are being used in the commercial battery charger ICs, such as linear chargers and switching-based regulators. While both topologies have their own sets of tradeoffs, designers have to be familiar with the benefits, drawbacks and design concerns of each topology. Furthermore, due to the charging input could be from either power adapter or universal serial bus (USB), the cell phone battery charger must be capable of handling dual input sources. Table II shows the comparison between switching-based regulator and linear regulator.

TABLE II.

COMPARISON BETWEEN SWITCHING-BASED REGULATOR AND LINEAR REGULATOR

	Switching-based regulator	**Linear regulator**
Advantages	1. High efficiency 2. Small size	1. Simplicity and low cost 2. Faster transient response 3. Low noise
Disadvantages	1. More components count 2. V_{out} must be less than V_{in}	1. Poor efficiency 2. V_{out} must be less than V_{in}

1.2.2 Laptop charger system

A. System configuration

The power system of a laptop consists of an external power adapter, an internal dc-dc charger IC, battery pack and an individual subsystem dc-dc converter, shown in Fig 1.3.

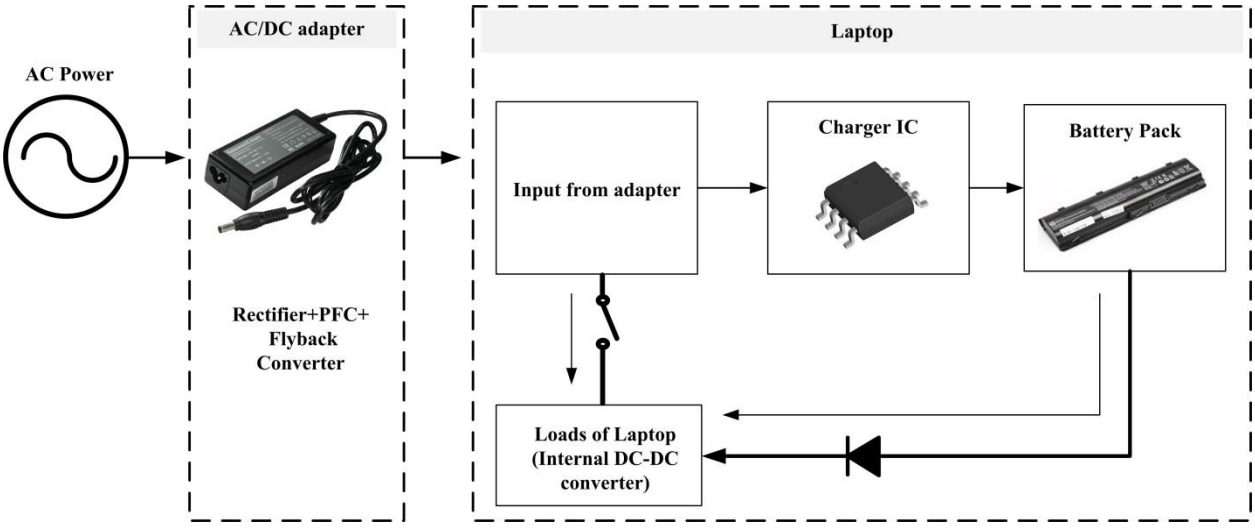

Fig.1.3. Laptop power battery system diagram

The ac adapter converts high voltage ac power from a wall outlet into a fixed low dc voltage. This is typically around 15-20V. The actual charging circuitry is inside of the laptop itself. The laptop contains many different sub-systems that all require their own individual regulated power; for example the drives use 5V and the memory use 3.3V. A non-isolated buck converter would be the most common topology of stepping down the high voltage to the required voltage. Power switch is used to select the source that powers the laptop. When the power from the ac adapter is available, the switch is on, the power goes into an internal dc-dc converter that will transform and regulate all of the required internal voltages. With ac input removed, the laptop runs from the battery, the power from the battery is fed back into the dc-dc converter.

The battery pack used in the laptop's market is generally from three to five series connected multiple Li-Ion batteries. The voltage range for a single Li-Ion cell is 2.7 minimum to 4.2V maximum [5].

B. Power adapter

The power adapter of the laptop is the fly-back converter followed by a diode rectifier with a capacitive filter shown in Fig.1.4(a). This configuration has been proved to be the most effective solution for power levels below 50W [6, 7]. However, the wide input voltage of the adapters can decrease the efficiency, because there is a wide variation of the voltage across the energy-storage capacitor. This drawback of the single-stage can be compensated by applying two-stage approach shown in Fig.1.4(b). Table III shows the comparison of the single stage and two stage charger. Besides, the power adapter design has to meet the IEC 1000-3-2 standard requirements (Limitation of Harmonic components)[8].

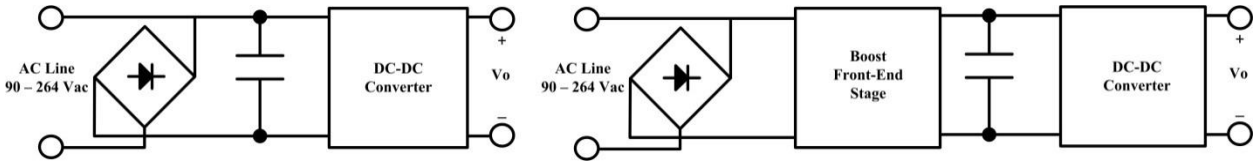

(a) (b)

Fig.1.4. Laptop power battery system diagram:
(a) single stage, (b) two stage

TABLE III.

COMPARISON BETWEEN SINGLE STAGE AND TWO STAGE CONVERSION

	Topology	Advantages	Disadvantages
Single stage	Fig.1.4(a)	Cost-effective, simple designed, and low part counts	Wide variation of the dc bus voltage, current harmonics and poor power factor
Two stage	Fig.1.4(b)	Well regulated dc bus voltage, reduce the size, unity power factor [9]	Control is complicated, higher part counts and high cost.

In the two-stage approach, the boost front-end stage well regulates the constant voltage on the capacitor, which not only lowering down the value and reducing the size of the capacitor but also improving the conversion efficiency of the dc-dc stage. Furthermore, the boost topology stage is also able to increase the power factor. Therefore, the two-stage approach has become the dominant charger topology for the laptop adapter in the market. Typically, the dc-dc converter used in the laptop adapter is fly-back dc-dc converter, shown in Fig.1.5, because the isolated-converter is capable of preventing the noise and harmonics from inserting to the system.

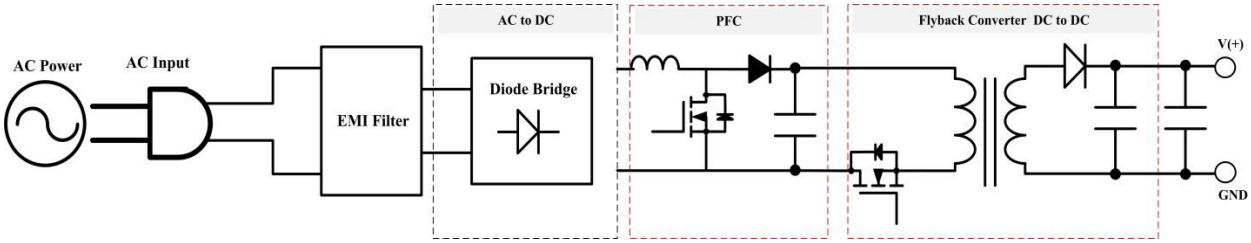

Fig.1.5. Two-stage laptop adapter with fly-back converter

1.2.3 EV battery charger system

A. Introduction

The role of battery energy is getting more significant due to the growing battery utilization of portable electronic devices, renewable energy sources, EVs and so on. Among them, EVs are the most popular alternative energy option in the reduction of oil consumption. A large portion of the

oil consumption is due to the transportation with most of the consumption being caused by road vehicles. The oil consumption consumed by transportation is expected to be increased up to 55% by 2030 according to the international energy outlook report [10]. Hence, alternative vehicle technologies related to reducing oil consumption has been explored and investigated. Plenty of different types of EVs have been developed nowadays, such as Plug-in Hybrid Electric Vehicles (PHEVs), Battery Electric Vehicles (BEVs) and Fuel Cell Electric Vehicles (FCEVs). The development of PHEVs and BEVs has become promising and gained interest from the automotive industry and customers, plenty of research has been investigated. Furthermore, compared to liquid carbon energy transportation, storing energy electrochemically in batteries is a reliable and cleaner way of storing transportation energy. Since EVs are powered by large battery pack that need to be charged from either an external power source or directly from the grid, their batteries, charging topologies and charging methods are gathering more attention. This thesis will be focusing on battery charging system for BEVs and PHEVs.

B. System configuration:

The system architecture of EV is shown in Fig.1.5 [11], the system consists of several modules to build the drive train and energy storage system.

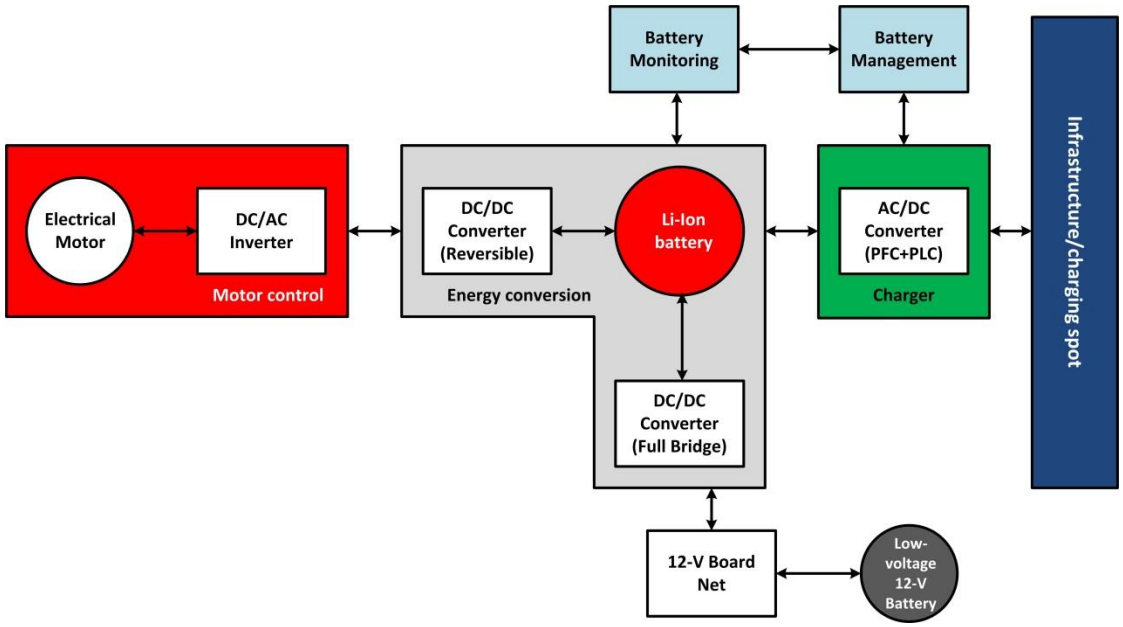

Fig.1.5. System structure of HEV/EV [11]

EV batteries require more attention to take care of regarding the safety issue since high amounts of delivered power would cause heat generation [12].

C. Classification of EV Chargers

Since the inception of the first EVs, there have been many different charging systems proposed. The chargers that can be classified based on their features and applications such as circuit topologies, location of the charger, connection type, waveform and direction of power flow. Table IV [13] shows the charger classification.

TABLE IV.
BATTERY CHARGER CLASSIFICATION [13]

Classification type	Options
Topology	Dedicated/ Integrated
Location	On-board/ Off-board
Connection type	Conductive/ Inductive/ Mechanical
Electrical waveform	AC/DC
Direction of power flow	Unidirectional/ Bidirectional
Power level	Level 1/ Level 2/ Level 3

Currently, the majority of EVs are designed with on-board unidirectional batteries charging systems. Besides the on-board batteries charging systems, some vehicles allow the charge of their batteries with off-board chargers. An on-board battery charging system refers to a charger implemented inside the vehicle. This type of charger is connected to the ac electrical grid voltage and is used to slowly charge the batteries. On the other hand, an off-board battery charging system is implemented outside the vehicle. It is given access to the dc voltage of the batteries and is used to charge the batteries as fast as possible – it is denominated as "fast charging". Table V illustrates the features of both types of chargers.

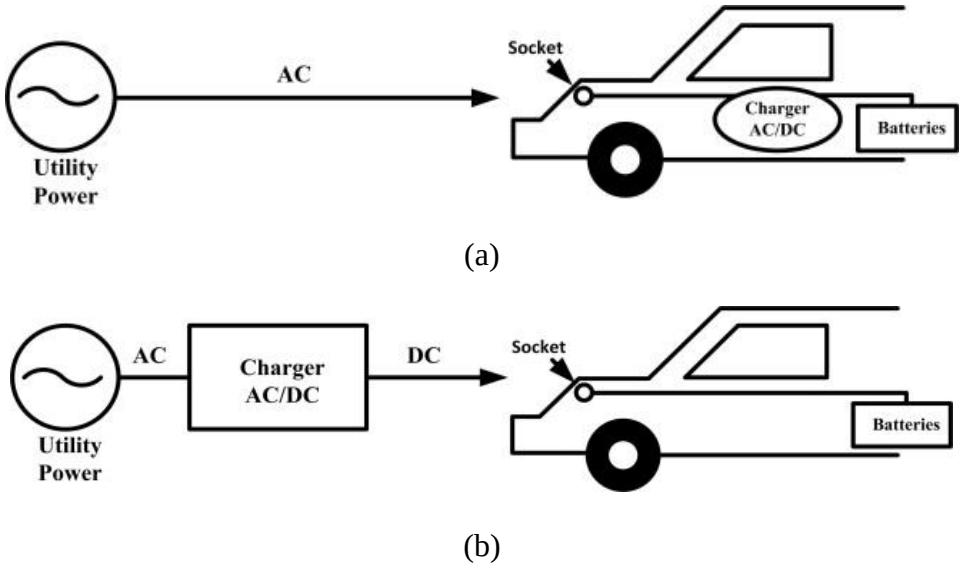

Fig.1.6. Configuration of EV charger: (a) on-board charger, (b) off-board charger

TABLE V.

COMPARISON OF ON-BOARD AND OFF-BOARD CHARGERS

	On-Board charger (Level 1&2)	Off-Board charger (Level 3)
Advantage	1. Flexibility (AC→DC) 2. Less concern about battery heating	1. Higher kW transfer 2. Fast charging→large current value 3. Reduces weight from vehicle 4. DC→DC
Disadvantage	1. Lower KW transfer 2. Adds weight to vehicle 3. Slow charging→ small current value	1. More sophisticated BMS systems 2. Inflexibility 3. Expensive

Regarding the way of connection to the vehicle, there are three different approaches: conductive, inductive and mechanical. The conductive batteries charging system is made through a physical contact between the vehicle and the power grid. In counterpart, with the inductive batteries charging system there is no physical contact but with high frequency transformer connects the vehicle to the power grid. Mechanical charging replaces the deficient battery pack with a full one in battery swap stations.

The charger can deliver power in either unidirectional way by just charging the battery, which is also known as grid-to-vehicle (G2V) or bidirectional way by receiving power from the grid and delivering power to the grid, which is known as vehicle-to-grid (V2G). More advanced designs introduce bidirectional power transfer [14].

International Electrotechnical Commission (IEC) has classified charging station into three categories based on power level [15]. Level one and two are small on-board battery chargers with an output maximum power of 3.3kW and 14.4kW, respectively. Level three charging stations are publicly used as fast charging stations with a maximum charging power from 50 to 240kW, which can charge the EV batteries to 80% level within 15 minutes and to a 100% level

within 30 minutes [16]. The following table VI shows the detailed description of the charger with respect to their power level.

TABLE VI.
CHARGING POWER LEVELS [17]

Power Level Types	**Charger location**	**Typical Use**	**Energy Supply Interface**	**Expected Power level**	**Charging Time**	**Vehicle Technology**
Level 1 **$120V_{ac}$ (US)** **$240V_{ac}$ (EU)**	On-board 1-phase	Charging at home or office	Convenience outlet	1.4kW (12A) 1.9kW (20A)	4-11 Hrs 11-36 Hrs	PHEV EVs
Level 2 **$240V_{ac}$ (US)** **$400V_{ac}$ (EU)**	On-board 1 or 3 phase	Charging at private or public outlets	Dedicated EVSE	4kW (17A) 8kW (32A) 19.2kW(80A)	1-4 Hrs 2-6 Hrs 2-3 Hrs	PHEVs EVs EVs

1.2.4 BESS battery charger system

A. Introduction

The power conditioning systems, including inverters and dc-dc converters, are often required for the BESS in order to supply normal customer load demand or send electricity into the grid. The most unique aspect to power electronics for energy storage is that they must be bidirectional, that is both taking power (during charging) and providing power (during discharge) from/to the grid. Unlike PV and fuel cell inverters, however, BESS inverters are not expected to consider the peak power operations. They only provide the power level demanded by the system that can be sustained by the battery [18].

The battery energy storage system can provide flexible energy management solutions that can improve the power quality of renewable-energy hybrid systems. The followings are the

benefits of the BESS

1. Compensates for intermittency of renewable energy, such as wind and solar.
2. Enables commercial and residential owners to cut energy cost.
3. Provide emergency power to the grid during the outages.
4. Act as a compensator to support reactive power to improve the power factor of the grid network.
5. Helps grid system operators maintain constant frequency.

Additionally, the battery storage system is very common to use with other types of energy sources in form of hybrid systems. When using with renewable sources, such as wind or PV, the BESS can offset the daily and seasonal intermittency of the primary energy, smooth-out load fluctuations, damp out utility transients, and facilitate islanding operation.

B. System configuration:

It must be noted that for BESS applications, the dc-dc and dc-ac converters must be bi-directional. The dc-dc converter may be necessary either to provide additional regulation for battery charge/discharge control or to regulate a specific dc voltage/current for the dc-ac converter. On the output, a filter consisting of passive components is used to mitigate high-frequency harmonics in the currents delivered to the transformer. Finally, an isolation transformer is used to step up the ac voltage and to provide isolation between the utility and the BESS. A typical filter topology is the LCL filter which is a third-order, low-pass filter connected between each phase. The dc-ac converter is referred to as a voltage source inverter (VSI). [18]

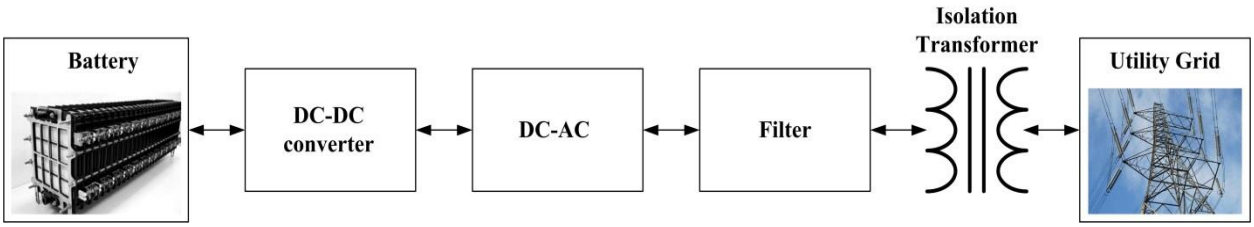

Fig.1.6. Building blocks of BESS power conditioning system (grid-tie BESS)

1.2.5 Battery charging approach

Typically, the lithium-Ion battery cells are expected to be the technology of energy storage for coming battery-powered systems because of high energy density, relatively low self-discharge and no memory effect [19]. The common charging techniques in the industry for lithium-Ion batteries are constant current constant voltage (CCCV) charging due to its simple-design, low cost and safe operation [20-22]. During CC mode, the current is regulated at a constant value until the battery cell voltage reaches a threshold voltage level. Then, the charging is switched to CV mode, and the battery is charged with a trickle current applied by a constant voltage. Fig.1.7 illustrates the charging curve of CCCV charging profile.

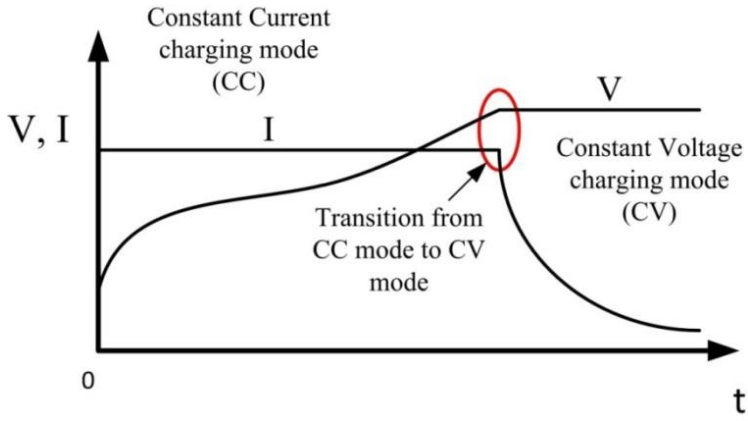

Fig.1.7. CCCV charging profile

Therefore, chargers and charging profile play an important role in the battery-powered systems. Nowadays, due to the growing market of rechargeable battery, the demands for high performance battery energy storage systems are increased. These demands are as follows: a) high charging efficiency, b) fast charging and c) long life cycle.

In order to achieve these demands, many of high performance battery charging algorithms have been developed such as fuzzy-control, neural network, genetic algorithm and model predictive control [23-26]. Recently, the sinusoidal ripple current (SRC) charge method shows remarkable performance because SRC charge method can not only enhance the battery charging performance by minimizing the impedance of batteries, but also reduce the temperature rise [27-30]. However, in order to perform SRC charging approach, it is necessary to have high performance hardware that is capable of generating a sinusoidal ripple waveform with precise frequency and magnitude control. Furthermore, the optimal charging frequency is determined by swept frequency. Therefore, the converter and the controller should have high bandwidth control capability.

1.3 Problem Statement

Since the existing CCCV charger system is designed in low frequency or dc current control, the bandwidth of the system is already determined. However, wide bandwidth is necessarily required for variable frequency control to perform SRC charge method. Nowadays, many advanced charging algorithms have been investigated to solve the aforementioned issue, such as pre-tuning PI control, adaptive sliding model control and model reference adaptive control

[38-40] have been investigated to enhance the battery charging system performance. However, some of these advanced approaches are too complicated to implement in commercial applications. In addition, some approaches require additional design or components to perform their charging algorithm.

1.3.1 Hardware limitations

The SRC charging method is necessary to have high performance hardware that is capable of generating a sinusoidal ripple waveform with precise frequency and magnitude controls. The conventional Lithium-Ion battery charger system is limited to perform SRC, due to the system's power switch or passive components were designed for low frequency and high power applications.

1.3.2 Bandwidth issue

To determine the optimal ripple current frequency in SRC charge method, frequency sweep function is required. Therefore, the converter and the current controller should response quickly with high bandwidth control capability. In order to satisfy aforementioned requirements, the existing CCCV charger systems is limited, because the CCCV charger systems, which use a fixed PI gain controller, are mostly designed in a low control bandwidth condition due to the charging current reference is low frequency or constant [31-33]. In order to apply SRC method to the conventional charger, the charger should be capable of tracking the input variable frequency reference. Therefore, the fixed PI gain control is limited to regulate wide range frequency of ripple current. Fig.1.8. demonstrates the requirements of the battery charger with respect to

CCCV method and SRC method.

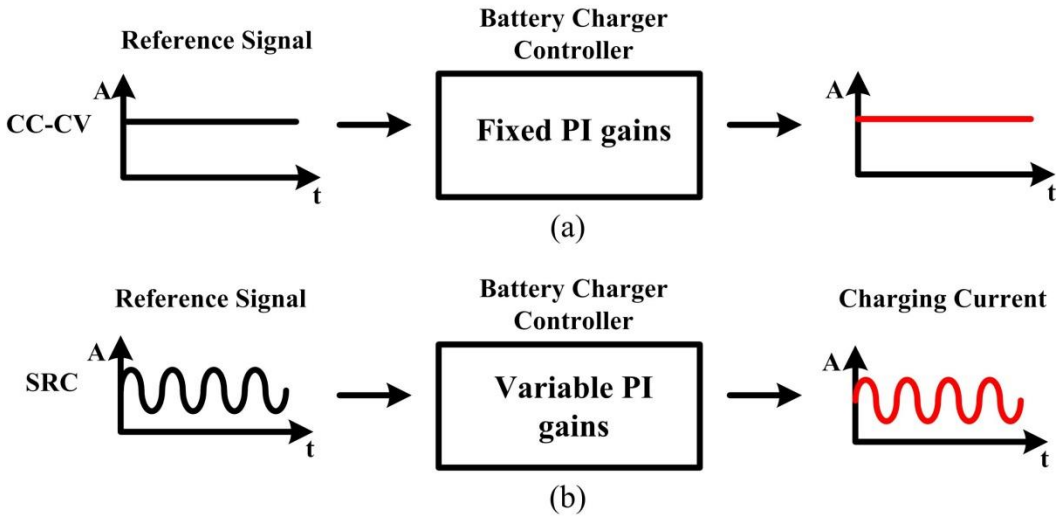

Fig.1.8. Difference between CCCV charging and SRC charging:
(a) CCCV charging, (b) SRC charging

1.4 Proposed Method

This thesis proposes the adaptive PI gain control based on Model Reference Adaptive Control (MRAC) to regulate variable frequency of charging ripple current. MRAC shows simple and good performance to adjust PI compensator gain with respect to a variable frequency reference [34]. The proposed approach is realized in a designed synchronous buck battery charger without any change in the switching devices and passive components. In addition, based on a variable structure model, MRAC controls the system with adaptation algorithm, which makes the system more flexible and regulated. The proposed model of the adaptive PI gain control based on MRAC with synchronous buck charger system is shown in Fig.1.9.

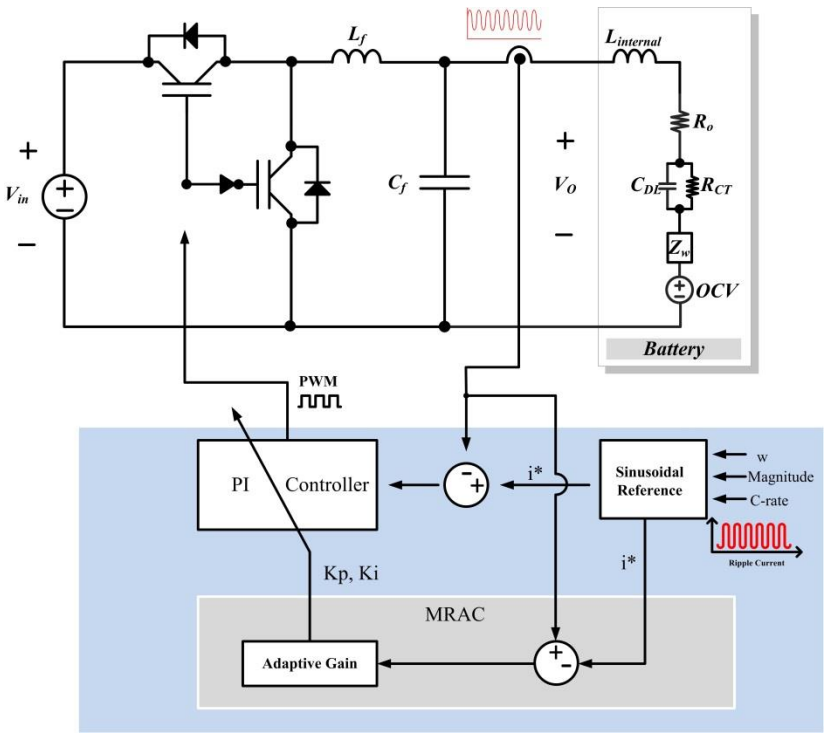

Fig.1.9. Proposed charging system with adaptive PI gain control based on MRAC

1.5 Thesis Organization

The thesis proceeds as follows. Chapter II reviews onboard battery charger systems, including the topology and operation of EV charger system. Chapter III illustrates the detailed system specifications and analysis of the existing battery charger system. In order to demonstrate the SRC charging method could be adopted in the existing charger system, the model of battery charger based on synchronous buck converter was designed and simulated in Chapter IV. The proposed approach is discussed with regard to the hardware and bandwidth limitations in Chapter V. In Chapter VI, the design of the MRAC for SRC charging approach is discussed, and the simulation and experimental results are presented. Chapter VII summarizes and concludes the thesis.

II. LITERATURE REVIEW

2.1 Review of the current EV charger system

There are a plenty of battery charger systems from low power to high power scale that have been discussed in chapter I. Since the EV's technology has revolutionized the whole transportation market and the renewable energy, and the hardware limitation of the proposed system is similar to EV charger. Therefore, this session would investigate this growing battery charger system.

2.1.1 Charger system

The charging time and lifetime of the battery have a strong dependency on the features of the battery charger [35]. The onboard dedicated charger is the power conversion equipment that connects the vehicle battery to the grid and the charge method determines safety and how fast does the battery get charged. From the structure point of view, typical EV battery on-board charger consists of an ac-dc rectifier to generate a dc voltage from the ac line followed by a dc-dc converter to generate the dc voltage or current required by the battery pack [36]. The isolated dc-dc converter or battery charger stage converts a dc source for the specific battery needs of EVs. Fig.2.1 demonstrates a typical two-stage on-board dedicated charger.

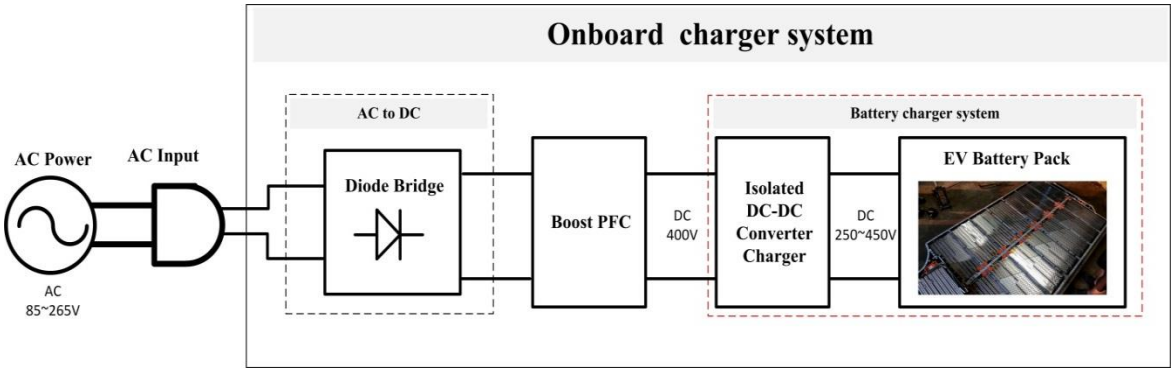

Fig.2.1. Topology of typical two-stage on-board dedicated charger system

Conversely, in integrated chargers, the traction inverter drive can serve as the charger at the same time when the vehicle is not working and plugged into the grid for charging. The common circuit applied in traction and charging may be the drive inverter, the dc-dc converter, or both. Hence, the integrated design saves the space and weight required of the power conditioning circuit as well as the cost. In addition, utilizing the already available traction drive, the charging time can be reduced [37]. On the other hand, most integrated chargers suffer the increased line current THD which is caused by using the motor winding reactance as the input filter of the rectifier circuit. In addition, dedicated chargers have better efficiency compared to integrated chargers. However, the dominant topology in EV's market is one of the extensions of the integrated charger- AC propulsion integrated charger. The examples of using this topology are BMW Mini E [37] and Tesla [38].

(a)

(b)

Fig.2.2. (a) BMW Active E (b) Tesla Roadster

Even both topologies have different operation in converting the ac power to dc link, they all require dc-dc converter stage to provide the certain and regulated power to charge the battery pack. There are three commonly used topologies for the dc-dc charger such as buck converter,

boost converter and buck-boost converter. It is necessary to understand the principle of operation of these converters [39]. Fig.2.3 shows individual converter scheme.

1. Buck operation: The current direction is from V_d to V_o and $V_d > V_o$. During the period that M1 is conducting, $t_{on} = DT_s$, inductor is charged and when M1 is off ($t_{off} = T_s - t_{on}$) inductance current will flow through diode M2.
2. Boost operation: The current direction is from V_o to V_d and $V_d > V_o$. . During the period that M2 is conducting, $t_{on} = DT_s$, inductor is charged and when M2 is off ($t_{off} = T_s - t_{on}$) inductance current will be discharged through M1.
3. Bidirectional buck-boost operation: The current direction is from V_d to V_o in buck mode and from V_o to V_d in boost mode. Changing the position of L and M1 changes the topology of buck-boost converter to boost-buck converter.

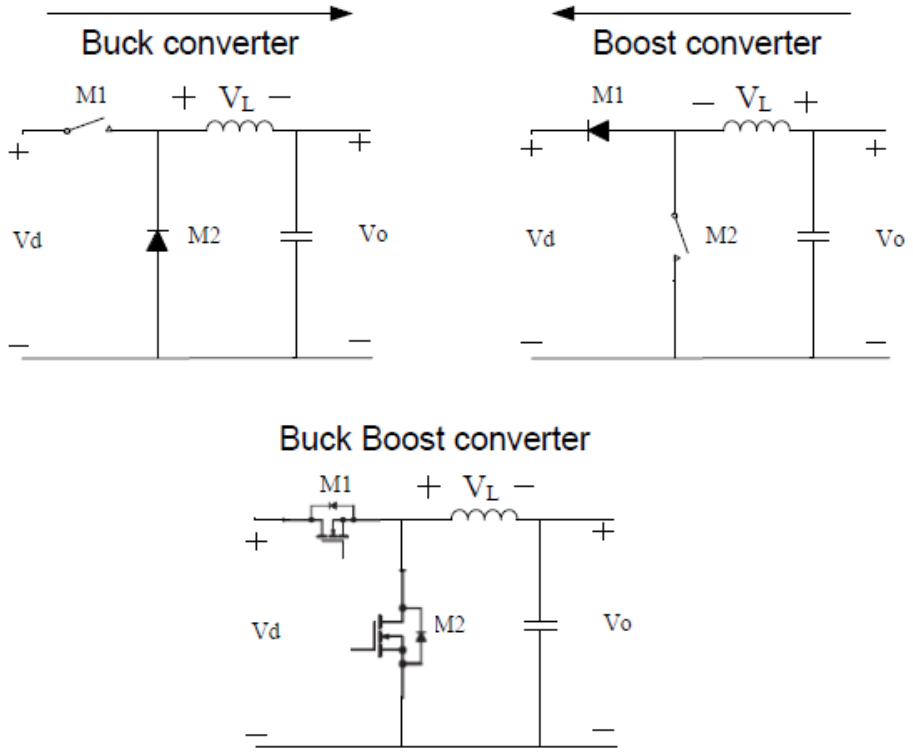

Fig.2.3. Buck, boost and bidirectional buck-boost converter scheme [35]

The CCCV charging method is used for charging for the EV's battery charger system, due to the commercial EV adopt Li-Ion battery as their energy storage system. Therefore the hardware design such as LC filter and the control bandwidth of existing dc-dc battery charger is only applicable for the low frequency or constant dc current charging.

2.2 Review of variable gain control method

The conventional CCCV charger system's bandwidth is limited to perform SRC charging method due to the hardware design. Since the system is required to generate full range sinusoidal ripple waveform with precise frequency and magnitude control to perform SRC charging method, the fixed PI control scheme is restricted. There are several advanced control approaches that have been investigated to deal with the bandwidth restrictions or the input is a variable frequency signal. Such as pre-tuning of PI controller, the adaptive sliding mode control (SMC) using simple adaptive control (SAC) and model reference adaptive control (MRAC). Details of these three methods will be discussed in 2.2.1-2.2.3.

2.2.1 Pre-tuning and adaption of PI controllers

The operation of this method is by taking advantage of phase-frequency estimator to generate a sine-wave $A\sin w_0 t$ (w_0 is adjustable frequency), then the desired w_0 and phase $\Phi_d$could be obtained by comparing the phase difference between the generated and measured sine-wave. After that, we are able to get the desired PI controller with the desired w_0 and the objective P gain and I gain could be obtained. The following Fig.2.4 shows the block diagram of this control method [40].

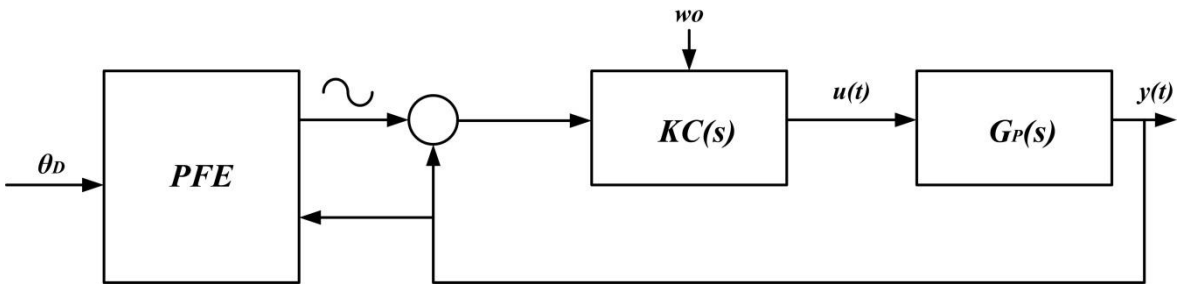

Fig.2.4. Block diagram of closed-loop PI tuner [40]

Indeed, this method can cope with the variety of transfer functions associated with typical process plant. And model the plant only at a carefully chosen frequency point, involves only minimal supervision. However, the additional design of the injection of a perturbing sinusoidal signal is required.

2.2.2 Adaptive sliding mode control using simple adaptive control

Adaptive SMC was considered a good method in dealing with the variable structure systems due to its capability to cope with the dynamic performance during load variations. However, in order to calculate the control input, the systems require additional equipment to sense or observe the outputs and the states of the power converters.

The author proposed an adaptive SMC using simple SAC developed for nonlinear systems with unknown parameters and dynamics. The role of SAC is to construct an equivalent control input of adaptive SMC. The sign function with a modified sliding surface is constructed in order to obtain a corrective control input. As long as we obtain the controlled signal, apply the PWM to control the output of the plant. This method uses the adaptive SMC strategy with SAC to eliminate the requirements of additional equipment for sensing or observing the states of the systems [41].

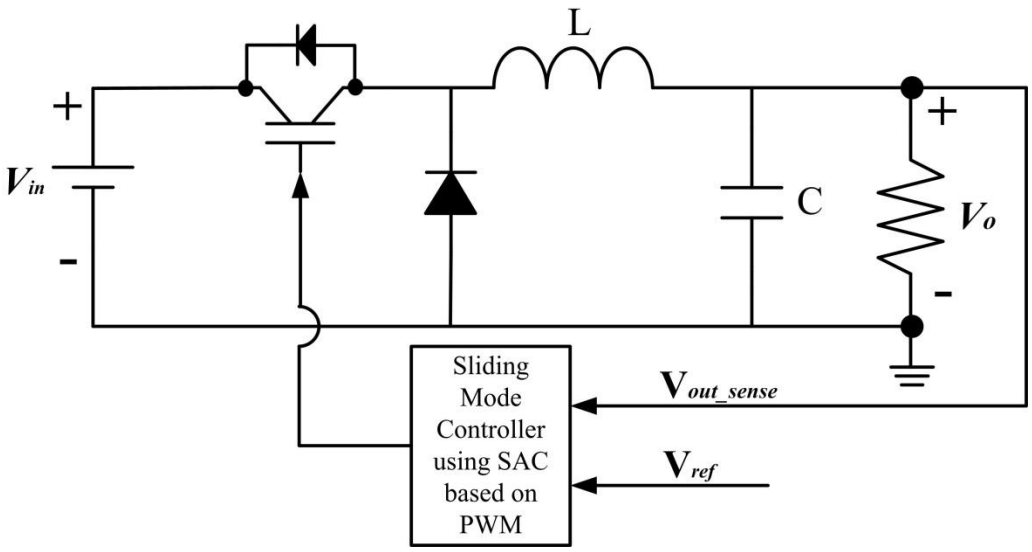

Fig.2.5. Control structure of a buck converter using an adaptive SMC with SAC [41]

2.2.3 Model Reference Adaptive Control

Adaptive control is one of the commonly used control strategies to design advanced control systems for better accuracy and performance. MRAC is a straightforward adaptive strategy with some adjustable controller parameters and an adjusting mechanism to adjust the control gains. There are many advanced control algorithms able to deal with the variable frequency input or the bandwidth limitation issues. However, some of them require either certain design aspect or complicated algorithm to implement. In comparison with the well-known and fixed gain PID controllers, adaptive controllers are more effective to deal with the unknown parameter variations and environmental affect. An adaptive controller consists of two loops, an outer loop or normal feedback loop and an inner loop or parameter adjustment loop [42].

The principle of MRAC is to adjust the controller parameters so that the output of the actual plant tracks the output of a reference model having the same reference input. Fig.2.6

demonstrates the MRAC system. And the each component's description is on table VII.

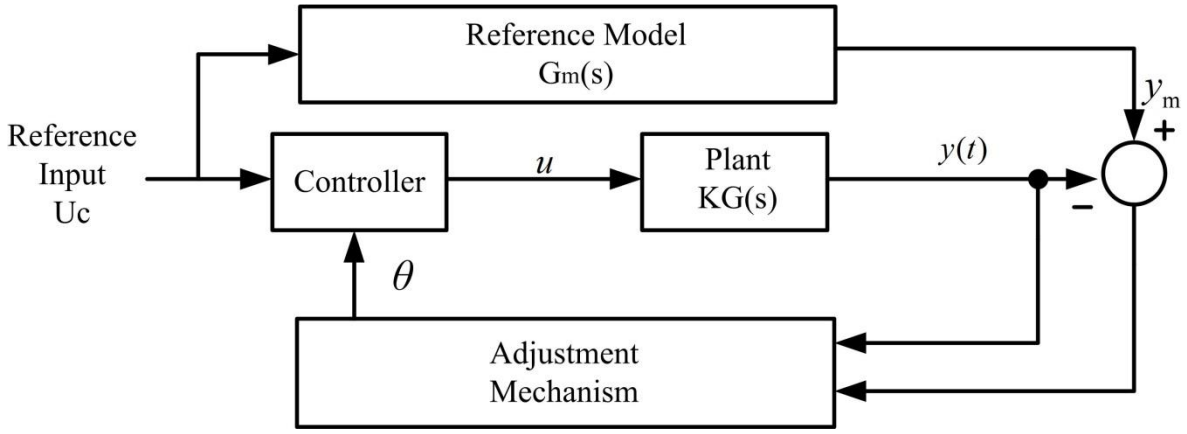

Fig.2.6. Block diagram of Model Reference Adaptive Control System [42]

TABLE VII.

COMPONENTS DESCRIPTION OF MRAC [40]

Reference Model $G_m(s)$	To provide the accurate and precise response of the adaptive control system to reference input.
Controller	It is usually described by a set of adjustable parameters. The value θ is the controller parameter.
Plant *KG(s)*	The system that is needed to be regulated.
Adjustment Mechanism	To adjust the controller parameters so that actual plant could track the reference model. Mathematical approaches such as Lyapunov theory, theory of augmented error and MIT rule can be used.

III. IMPACT ANALYSIS OF SINUSOIDAL RIPPLE CURRENT

3.1 System review

The synchronous buck converter is used to verify the proposed method. The hard switching based IGBT charger is designed and the switching frequency is 20 kHz with the second order LC filter. Originally, this charger system was designed for the CCCV charging method. The following topology, Fig.3.1, shows the synchronous buck converter operates in CCCV mode charging. In addition, the equivalent circuit diagram of a battery is also shown in Fig.3.1. A battery consists of internal inductance, L_f, resistance, R_O, charger transfer resistance, R_{CT}, double layer capacitance, C_{DL}, and Warburg impedance, Z_W [43].

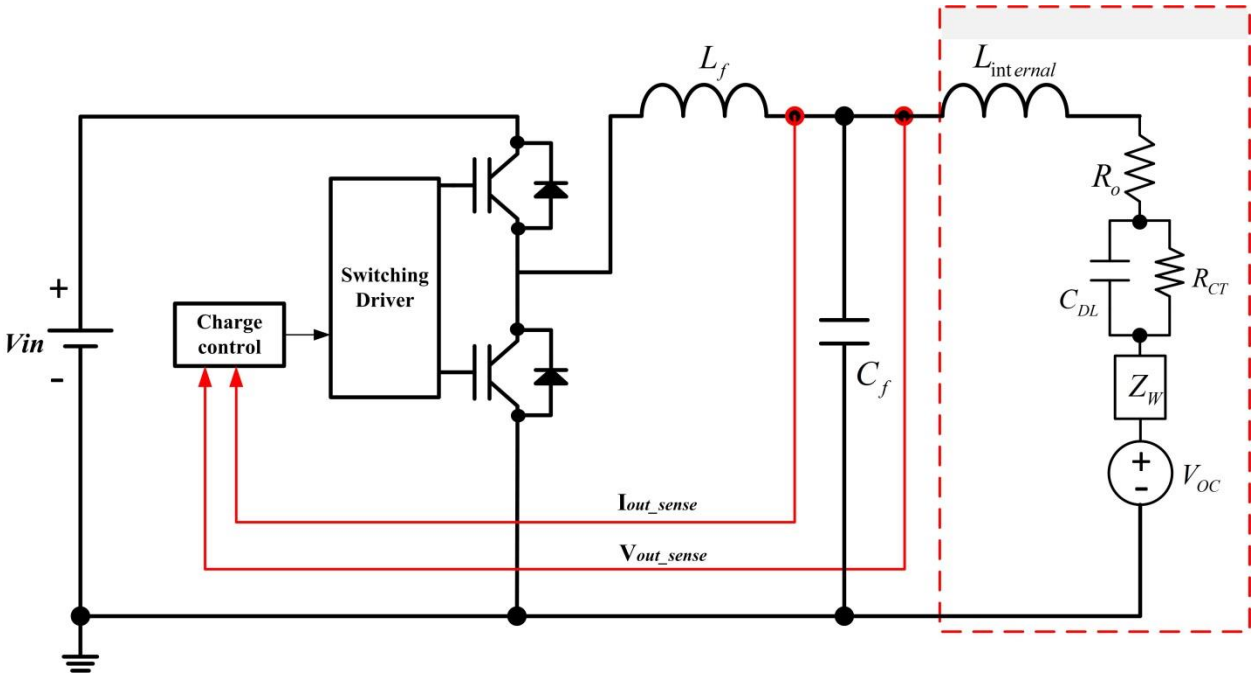

Fig.3.1. Synchronous buck charger in CCCV

3.1.1 Basic operation of synchronous buck converter

The basic operation of buck converter is discussed in chapter two; the term *synchronous* indicates that the power switch (MOSFET or IGBT) is used instead of a diode. Today's synchronous buck converter use pulse-width-modulation (PWM) as the operation mode. PWM holds the frequency constant and varies the pulse width (t_{on}) to adjust the output voltage. The average power delivered is proportional to the duty cycle, *D*, making this an efficient way to provide power to a load.

$$D = \frac{t_{on}}{t_{on}+t_{off}} \cong \frac{V_{out}}{V_{in}} \quad (1)$$

The power switches are controlled by a pulse-width controller, which uses either voltage or current feedback in a control loop to regulate the output voltage in responses load changes. Therefore, the principle of operation of the synchronous buck converter is similar to the regulator buck converter. Nevertheless, the synchronous buck converters show better performance and efficiency than the buck converter in all but in light load condition [44]. Since the inductor current in the buck converter flows only in one direction; however, the current is allowed to flow in both directions with the synchronous buck converter in light load case. Power is dissipated when reverse current flows.

3.2 System analysis and limitation

The second order low-pass filter characteristic of the output LC filter is designed to attenuate higher frequency components such as switching frequency and noise. A design rule of thumb is

to have the cut-off frequency, f_c, of the low-pass filter less than 10% of the switching frequency, f_s [45]. In second order low-pass filter design, the cut-off frequency is approximately matched the LC resonant frequency, f_o, hence, the calculation of the cut-off frequency of the LC filter is the same as the resonant frequency.

$$f_c \cong f_o = \frac{1}{2\pi\sqrt{LC}} \tag{2}$$

Typically, the 10-base rule is acceptable to determine the cut-off frequency of the LC filter [46]. It means that $10f_c$ is the -40dB point, and the original amplitude is attenuated by 1%, in this case, the high frequency ripple or noise could be greatly reduced. In addition, this rule is also applicable to determine the loop crossover frequency, because $f_c/10$ has no phase delay and gain, as shown in Fig.3.2. In addition, it is necessary that the loop crossover frequency be limited below the resonant frequency of the LC filter. Otherwise, a harmful oscillation occurs and a controller can be unstable [47]-[48].

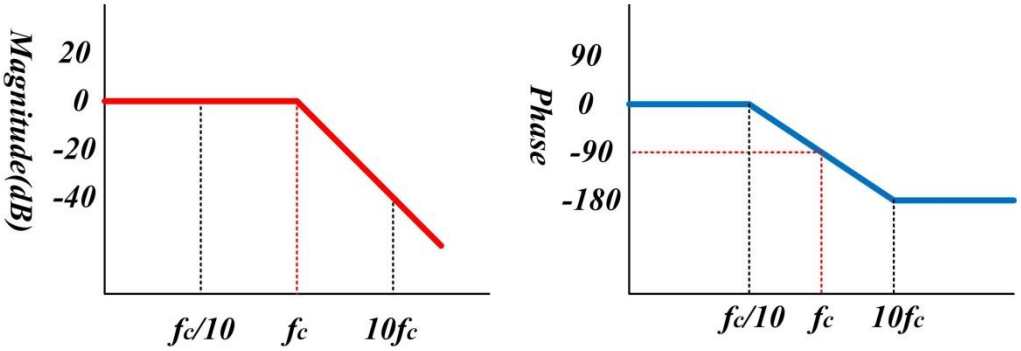

Fig.3.2. Bode plot of determination of the loop crossover frequency

Therefore, the cut-off frequency of the LC filter should be greater than the loop crossover frequency and less than the switching frequency.

The following shows the detail analysis of how to determine the range of the cut-off frequency. Since the conventional CCCV charging is a slow response system, the 10-base rule is well applicable for calculating the cut-off frequency and the loop crossover frequency of the compensator. If the switching frequency is 20 kHz, the cut off frequency of the low pass filter should be set to be at least lower than f_s/10 and the attenuation ratio should be considered. For example, to optimize the output filter performance, generally, the ripple current of inductor, I_L, is acceptable to be 20% of output current. If the output current is $15A_{dc}$, the ripple current of inductor will be $3A_{peak}$. By applying the 10-base rule, this $3A_{peak}$ will be $0.03A_{peak}$. In order to analyze this relationship, the switching frequency and quality factors are fixed at 20 kHz and 0.5, respectively. The reason to set quality factors, Q at 0.5 is that the system is said to be critically damped. Critical damping results in the fastest response possible without overshoot [49].

The magnitude of $G(jw)$ can be calculated as follows [48]:

$$\|G(jw)\| = \frac{1}{\sqrt{\left[1-\left(\frac{w}{w_o}\right)^2\right]^2+\frac{1}{Q^2}\left(\frac{w}{w_o}\right)^2}} \tag{3}$$

where w is the switching frequency, w_o is the resonant frequency of LC filter, and Q is the quality factor. Fig.3.3 shows the relationship between amplitude ratio and cut-off frequency.

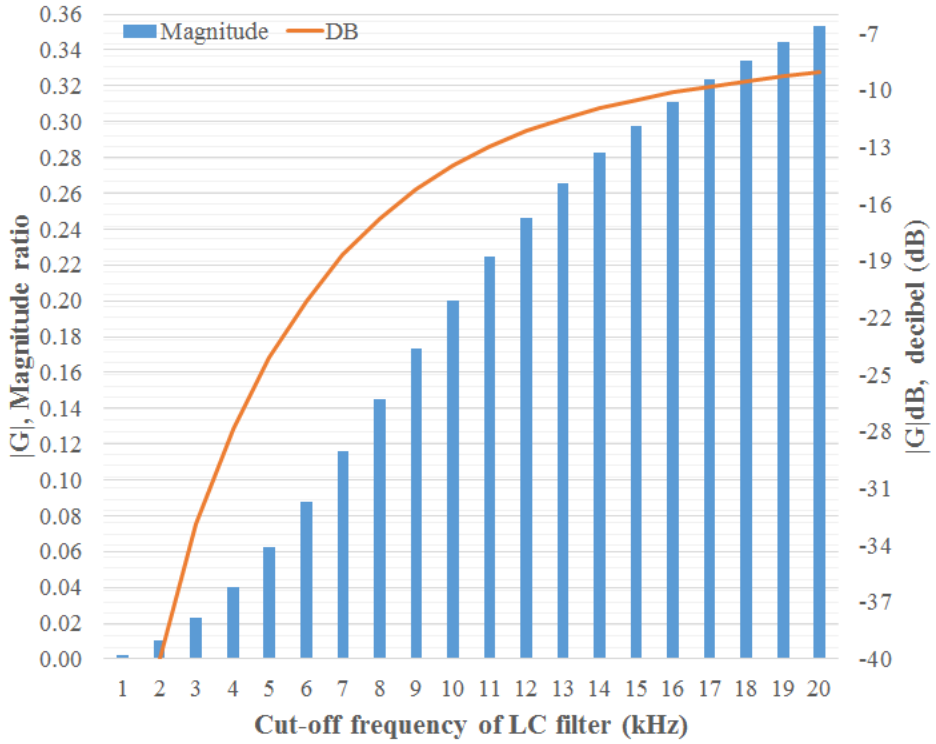

Fig.3.3. Relationship between switching frequency and cut-off frequency

The best way is to select the cut-off frequency of the LC filter at -40dB based on the switching frequency, which is about 2 kHz. If the ripple is acceptable to be attenuated by 15%, a higher cut-off frequency up to 8 kHz can be selected. Based on this relationship, the cut-off frequency can be determined as shown in Table VII. The theoretical cut-off frequency has a range from 2 to 8 kHz.

TABLE VII.

RELATIONSHIP BETWEEN SWITCHING FREQUENCY AND CUT-OFF FREQUENCY

Parameter	Symbol	Value	Unit
Switching frequency	f_{sw}	20	kHz
Optimal cut-off frequency	f_{c_opt}	2	kHz
Maximum cut-off frequency	f_{c_max}	8	kHz

3.3 Requirements of sinusoidal ripple current charging

In the aforementioned design procedure, we considered the range of cut-off frequency with respect to the analysis from the perspective of the switching frequency. In fact, to design a dc-dc converter for SRC charging, the swept frequency of the ripple current should be taken into account. The swept frequency has a range from 1 to 600 Hz in the proposed application and battery characteristics [50]. Importantly, it is also related to the loop crossover frequency. According to the previous explanation, the optimal cut-off frequency of the LC filter is 2 kHz. In this case, the control bandwidth of this filter is restricted to 600 Hz SRC regulation. Thus, the cut-off frequency of the LC filter needs to be adjusted base on the loop crossover frequency. The loop crossover frequency is assumed to be 600 Hz of ripple current frequency.

The cut off frequency should be about 3 times higher than the loop crossover frequency in the current-mode control [51]. Again, Q factor is assumed to be 0.5. As in the case of the real single pole, we could choose the slope of this asymptote to be identical to the slope of the actual curve at f = fc. It can be shown that this choice leads to the following asymptote break frequencies:

$$f_{crossover} = (e^{\pi/2})^{-\frac{1}{2Q}} f_{c\_min} \tag{4}$$

A better choice, which is consistent with the approximation 10-base rule used for the real single pole is:

$$f_{crossover} = 10^{-\frac{1}{2Q}} f_{c\_max} \tag{5}$$

The result is shown in Table VIII.

TABLE VIII.

RELATIONSHIP BETWEEN SWITCHING FREQUENCY AND CUT-OFF FREQUENCY

Parameter	Symbol	Value	Unit
Switching frequency	f_{sw}	20	kHz
Quality factor	Q	0.5	
Maximum cut- off frequency	f_{c_max}	6	kHz
Minimum cut-off frequency	f_{c_min}	2.9	kHz

Therefore, we could conclude that the desired cut-off frequency range can be determined by the Table VIII and Table IX. From the switching frequency perspective, the desired cut-off frequency is ranged from 2 kHz~8 kHz and from the loop gain crossover frequency perspective; the desired cut-off frequency is ranged from 2.9 kHz~6 kHz. However, since our objective is to be able to cope with the variable frequency signal from 1-600 Hz, the desired cut-off frequency should be beyond the range of crossover frequency but within 2 to 8 kHz. Fig.3.4 demonstrates the range of desired cut-off frequency based on Table VII and Table VIII.

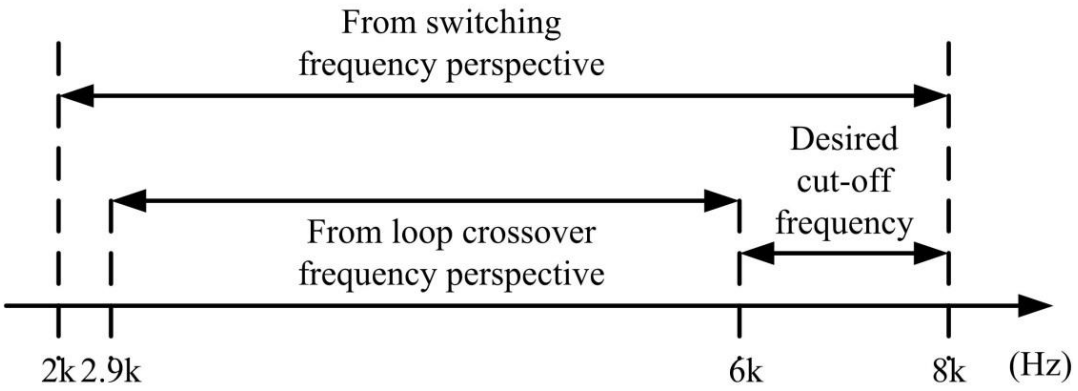

Fig.3.4. Diagram of determining desired cut-off frequency

IV. BATTERY CHARGER BASED ON SYNCHRONOUS BUCK CONVERTER

4.1 Design of Battery Charger

Originally, the filter inductance was 1.4mH and we added one more inductor with 0.615 mH in parallel in order to shift the LC filter resonant frequency to 7.7 kHz. The final inductance value is 0.43 mH. Theoretically, this value is acceptable because the range is within 6 to 8 kHz. The design resonant frequency satisfies the requirement to cover the cross over frequency. The Li-Ion battery used in the system is Valence U1-12XP, shown in Fig.4.1, the maximum input voltage for the battery is 14.6 V and the capacity is 40 Ah. In our case, the range of the current frequency provided to charge the battery is from 1~600 Hz and the charging current is set to be 15 A. The final design parameters of the battery charger system based on synchronous buck converter are in Table IX.

Fig.4.1. Valence U1-12XP Lithium-Ion Battery [52]

TABLE IX

SPECIFICATION OF THE BATTERY CHARGER

	Parameter	Symbol	Value	Unit
Sync-buck converter	Input voltage	V_s	50	Vdc
	Output voltage	V_O	14	Vdc
	Filter inductor	L_f	0.43	mH
	Filter capacitor	C_f	1	uF
	Switching frequency	f_s	20	kHz
	Cut-off frequency of LC filter	f_c	7.7	kHz
Li-ion battery	Variable frequency range	f_{var}	1~600	Hz
	Ohmic resistance	R_o	6.9	mΩ
	Charge transfer resistance	R_{CT}	1.2	mΩ
	Double layer capacitance	C_{DL}	2.6	F
	Battery voltage	V_{bat}	12.1~14.6	V

4.2 Transfer function of Battery charger

Commonly, the converter output characteristics are the same as a low pass filter. Thus, in a feedback system, the output is impacted by the frequency of model and input reference. Based on the specification of the battery charger, the plant model is designed as follows:

$$G(s) = \frac{1.726s^2+3.37s+1.645}{s^2+0.02211s-0.8873} \tag{6}$$

Since the system is designed based on digital control, the transfer function of the plant model has to be transferred to z domain by the sampling time, $50\mu s$.

$$G(z) = \frac{a_0z^3+a_1z^2-a_2z-a_3}{b_0z^3+b_1z^2-b_2z-b_3} \tag{7}$$

where $a_0 = 3.179$, $a_1 = 3.228$, $a_2 = 3.08$, $a_3 = 3.128$, and $b_0 = 1$, $b_1 = 0.9837$, $b_2 = 0.9993$, $b_3 = 0.9831$.

The open loop transfer function, LG(z), is as follows:

$$LG(z) = \frac{a_0z^4+a_1z^3-a_2z^2-a_3z+a_4}{b_0z^4-b_1z^3-b_2z^2+b_3z-b_4} \tag{8}$$

where $a_0 = 0.121$, $a_1 = 0.002359$, $a_2 = 0.2396$, $a_3 = 0.002343$, $a_4 = 0.1186$ and

$b_0 = 1, b_1 = 1.984, b_2 = 0.01561, b_3 = 1.981,\ b_4 = 0.9831.$

4.3 Control simulation and analysis

4.3.1 Bode plot

In Fig. 4.2, G(z) refers to the plant model, LG(z) represents loop transfer function and C(z) refers to the first order controller in z domain, respectively. From the following bode plot, we can realize that the cut-off frequency is shifted to 7.7 kHz. Since the crossover frequency is often approximated to be the bandwidth of the system, the designed bandwidth is 766 Hz, which is beyond the maximum input frequency, 600 Hz. Thus, this system is stable since the phase margin is positive and is around 90^o.

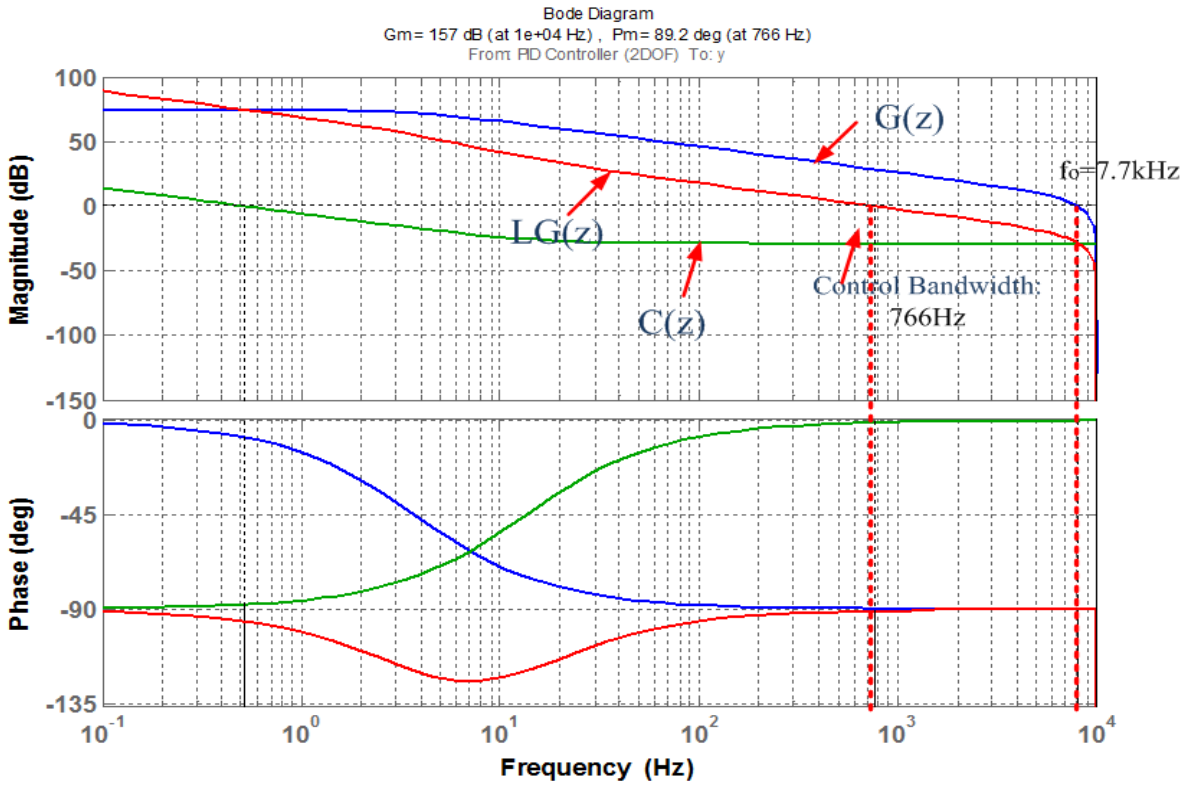

Fig.4.2. Bode plot with conventional fixed gain of PI controller

4.3.2 Nyquist diagram

Even though the cut-off frequency of the system was sufficiently designed, the system can still be unstable due to swept frequency effects. In order to analyze this impact, the frequency response estimation feature of MATLAB is used. The following Nyquist diagram, Fig.4.3, shows that if several sine waves of varying frequencies get involved, the system can lead to unstable conditions.

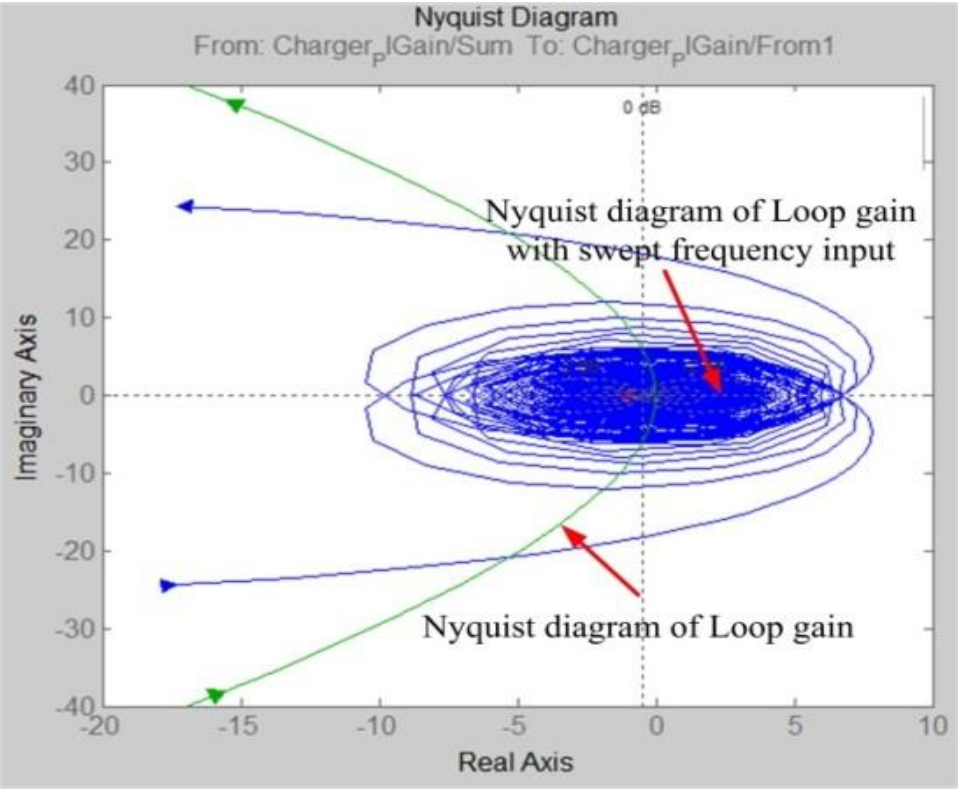

Fig.4.3. Nyquist diagram: model change by swept frequency input

V. APPLYING SRC TO THE CONVENTIONAL CHARGER

The cut-off frequency and the PI gain are the two factors that would affect the performance of applying SRC charging method to the conventional CCCV charger. The simulation results demonstrate how the performance could be affected by these factors.

5.1 Design of the test approach

The first test is the impact of cut-off frequency of LC filter. Typically, filter capacitance has no significant impact on the current control because our load is the battery which contains large size capacitance. In order to determine the controllability and stability conditions, the ripple current frequency is ranged from 1~600 Hz and the switching frequency is at 20 kHz. According to LC filter design, the cut-off frequency is 2 kHz. From the perspective of cross over frequency, the cut-off frequency is 6 kHz. In this point, above the switching frequency and the optimized frequency are analyzed. The filter inductance value is varied from 46.2uH to 6.33mH. The cut-off frequency of the LC filter is varied from 23.4 kHz to 2 kHz.

Table VIII shows the scenarios of eight conditions. Con# 1 describes the LC filter where the cut-off frequency is higher than switching frequency, whereas Con# 2 shows that these two frequencies are too close to each other. Both cases result in severe switching noise involved because the LC filter cannot filter out the high frequency components. Con# 3 to Con# 4 are the frequency region near -25dB and it results in overshoot and phase delay but the output current is stable and the noise is reduced. Con# 5 to Con# 8 shows that the output current at high frequency is uncontrollable. The results are shown in Table X and Fig.5.1.

TABLE X.
LC VALUE IMPACT OF THE SYSTEM

	L	C	fc	Description
Condition# 1	46.2uH	1uF	23.4 kHz	Severe switching noise involved
Condition # 2	0.2mH	1uF	11.3 kHz	Severe switching noise involved
Condition # 3	0.38mH	1uF	8.16 kHz	Overshoot and phase delay but stable and controllable
Condition # 4	0.43mH	1uF	7.7 kHz	Overshoot and phase delay but stable and controllable
Condition # 5	0.6mH	1uF	6.5 kHz	Uncontrollable from 500Hz
Condition # 6	0.7mH	1uF	6 kHz	Uncontrollable from 400Hz
Condition # 7	1.2mH	1uF	5 kHz	Uncontrollable from 300Hz
Condition # 8	6.33mH	1uF	2 kHz	Uncontrollable from 100Hz

The second test is the impact of P gain and I gain change. In this case, the cut-off frequency of the LC filter is fixed at 7.7 kHz and the PI gains are varied. In order to compare the performance, the fixed high gain and fixed low gain are used as follows:

High fixed gain: kp = 7.5 and ki = 0.5

Low fixed gain: kp = 0.75 and ki = 0.05

From the high fixed gain condition, dc current is well regulated within bandwidth of the LC filter shown in Fig.5.2. However, the system is not able to track the reference signal at high frequency range. In the high fixed gain condition, the error percentage between the reference and the output feedback current is 6.8%. The result is shown in Fig.5.2.

In the low fixed gain condition, the error percentage is even worse, which is 32%. In addition, the overshoot increases and phase delay occurs at 200Hz. And the output current has attenuation and severe phase delay after 400Hz. After this, the controller cannot regulate the high frequency reference because the control bandwidth is too low to track the reference ripple current shown in Fig.5.3 (b).

5.2 Simulation Results

5.2.1 LC filter cut-off frequency

The following figures demonstrate the impact of the cut-off frequency of the LC filter on the system.

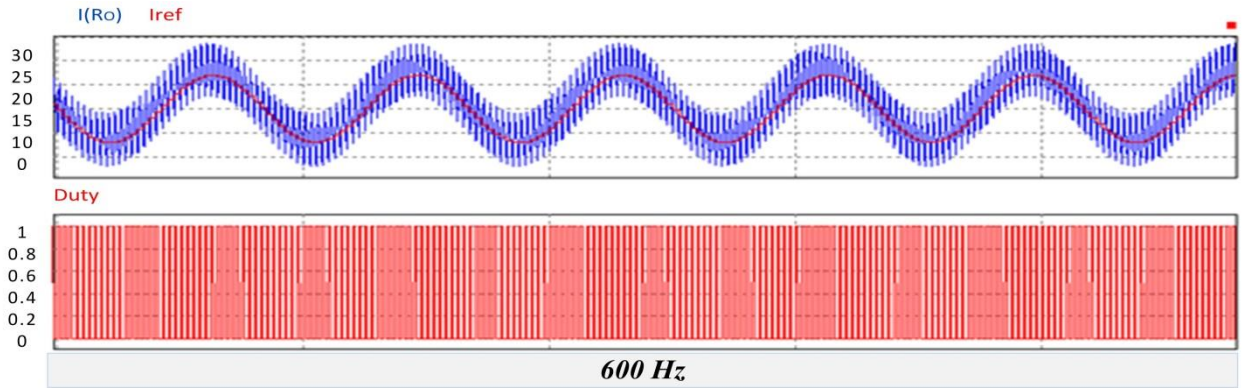

(a)

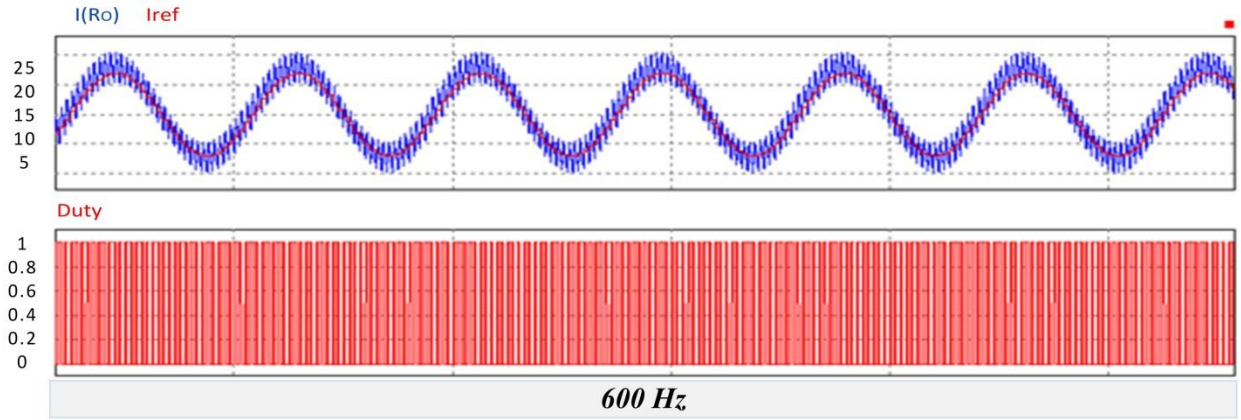

(b)

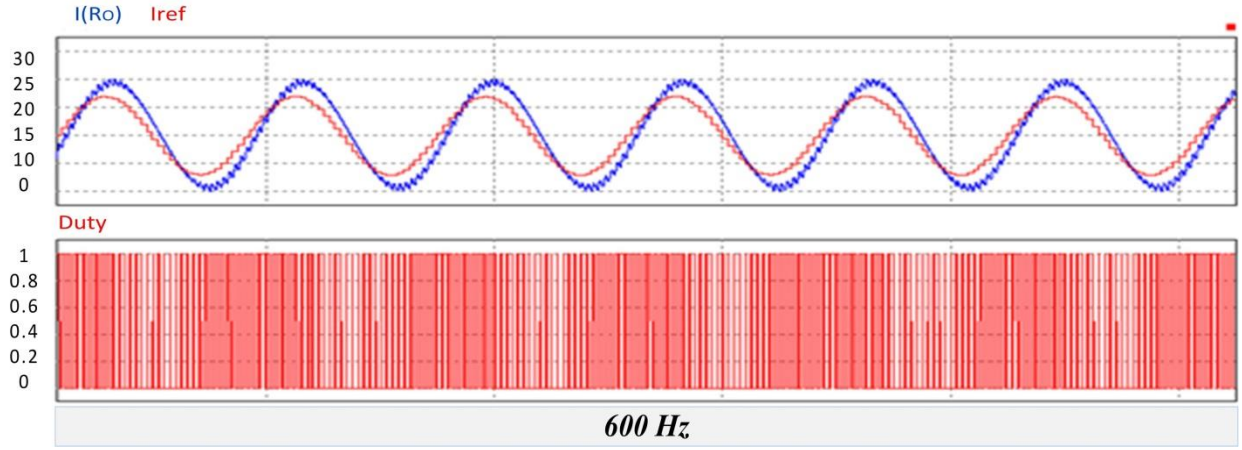
I(Ro)
Iref
30
25
20
15
10
0
Duty
1
0.8
0.6
0.4
0.2
0
600 Hz

(c)

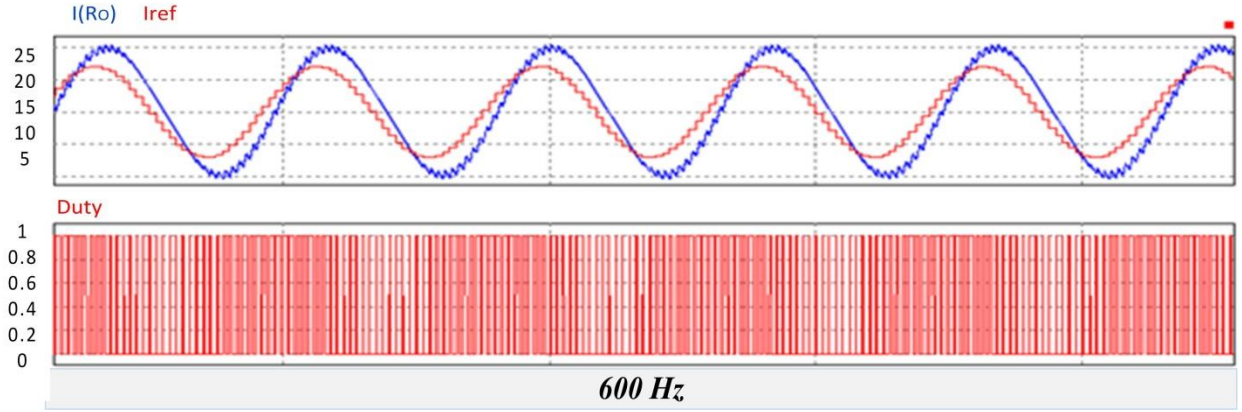
I(Ro)
Iref
25
20
15
10
5
Duty
1
0.8
0.6
0.4
0.2
0
600 Hz

(d)

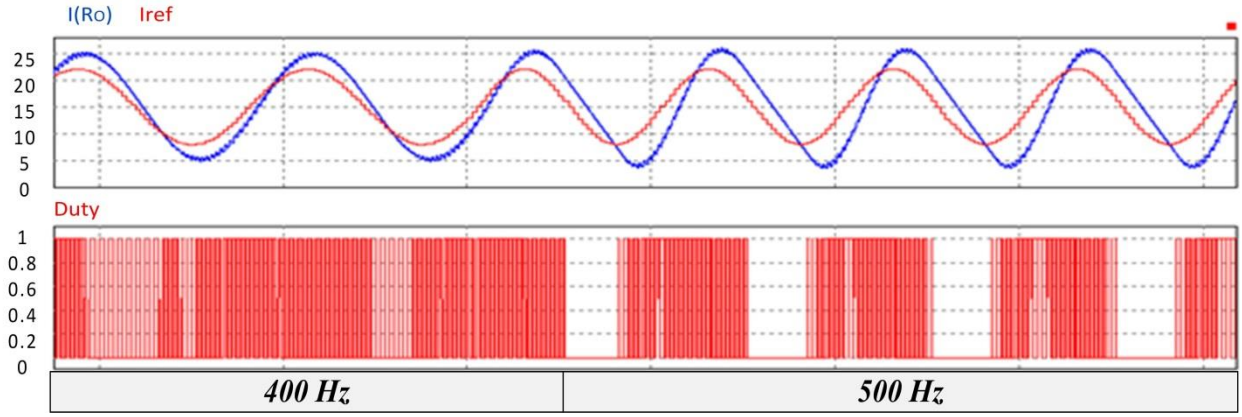
I(Ro)
Iref
25
20
15
10
5
0
Duty
1
0.8
0.6
0.4
0.2
0
400 Hz
500 Hz

(e)

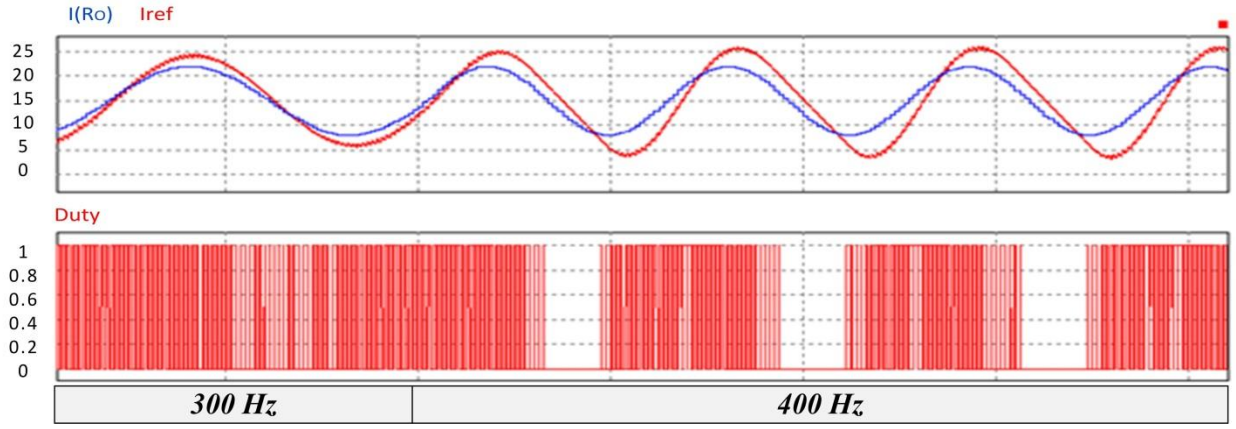

(f)

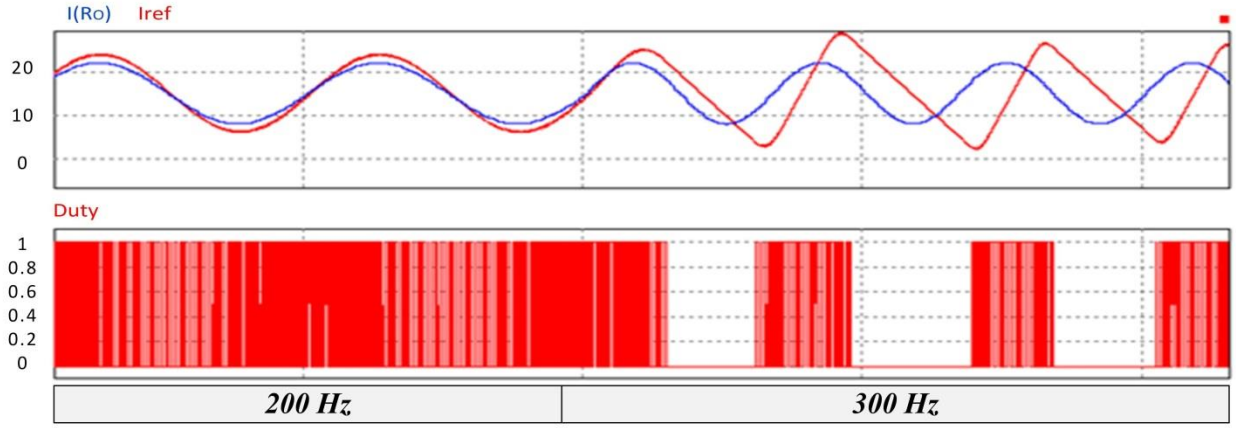

(g)

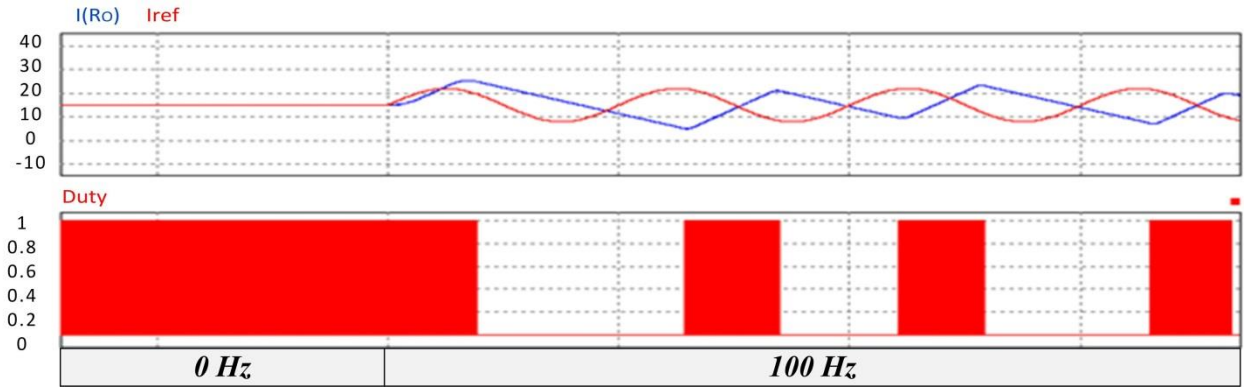

(h)

Fig.5.1 Impact of cut-off frequency on system:

(a) fc=23.4 kHz, (b) fc=11.3 kHz, (c) fc=8.16 kHz, (d) fc=7.7 kHz, (e) fc=6.5 kHz, (f) fc=6 kHz,

(g) fc=5 kHz, and (h) fc=2 kHz,

5.2.2 P & I gains change

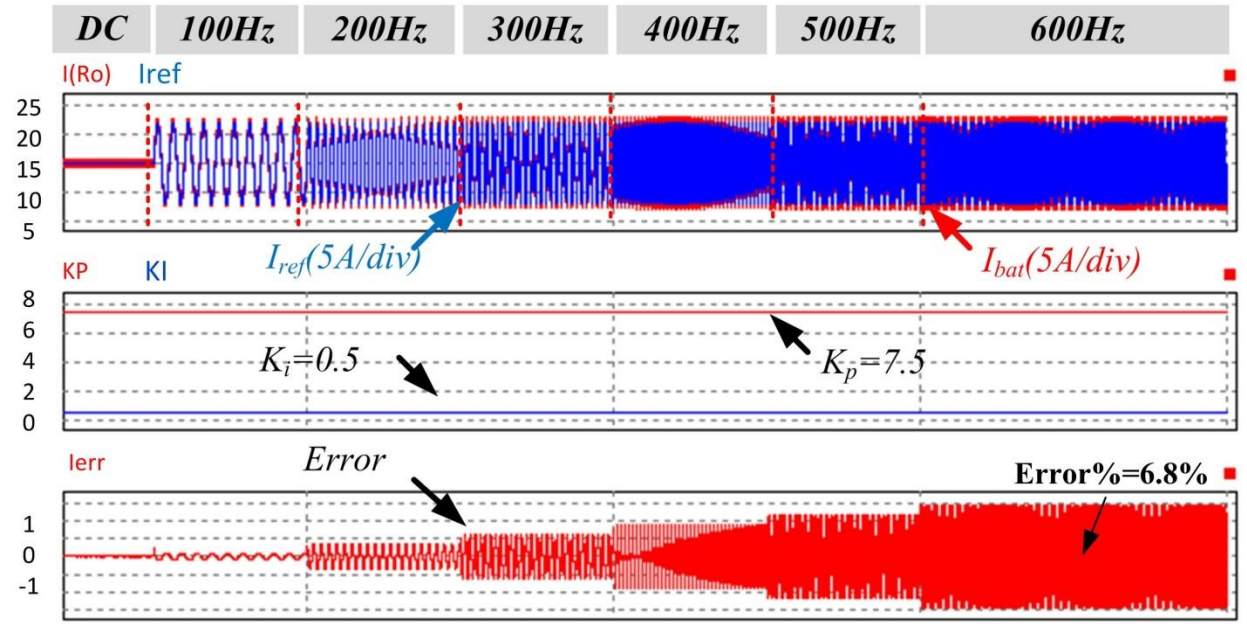

(a)

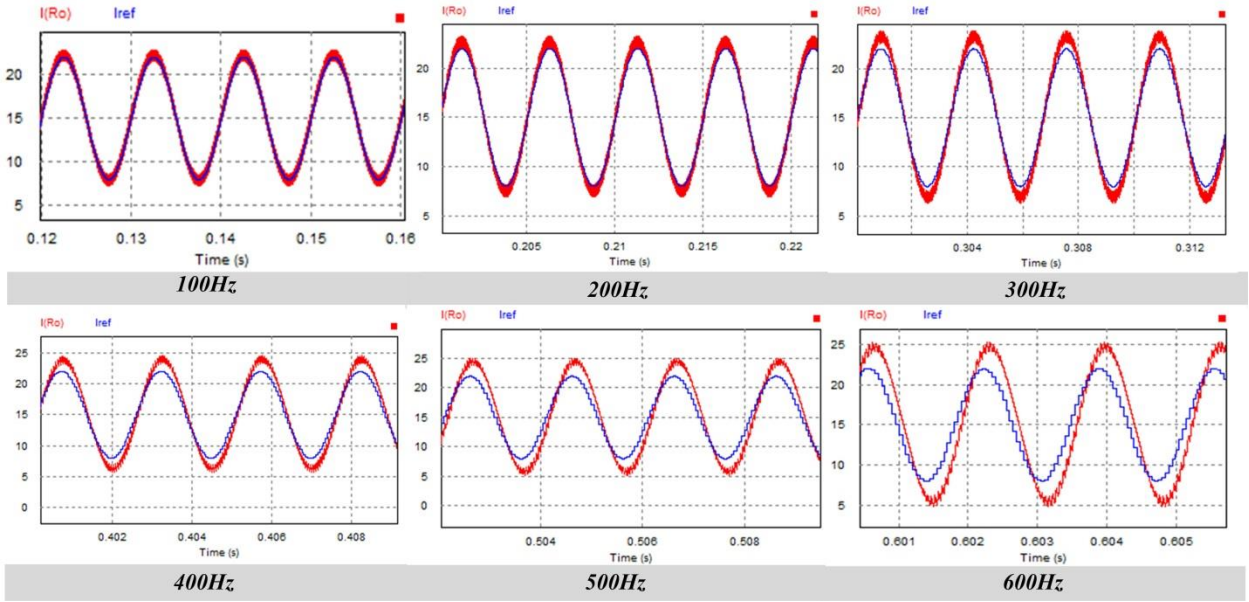

(b)

Fig.5.2. Fixed gains of PI controller: high fixed gain: (a) $K_p = 7.5, K_i = 0.5$, (b) waveform from 100 Hz~600 Hz

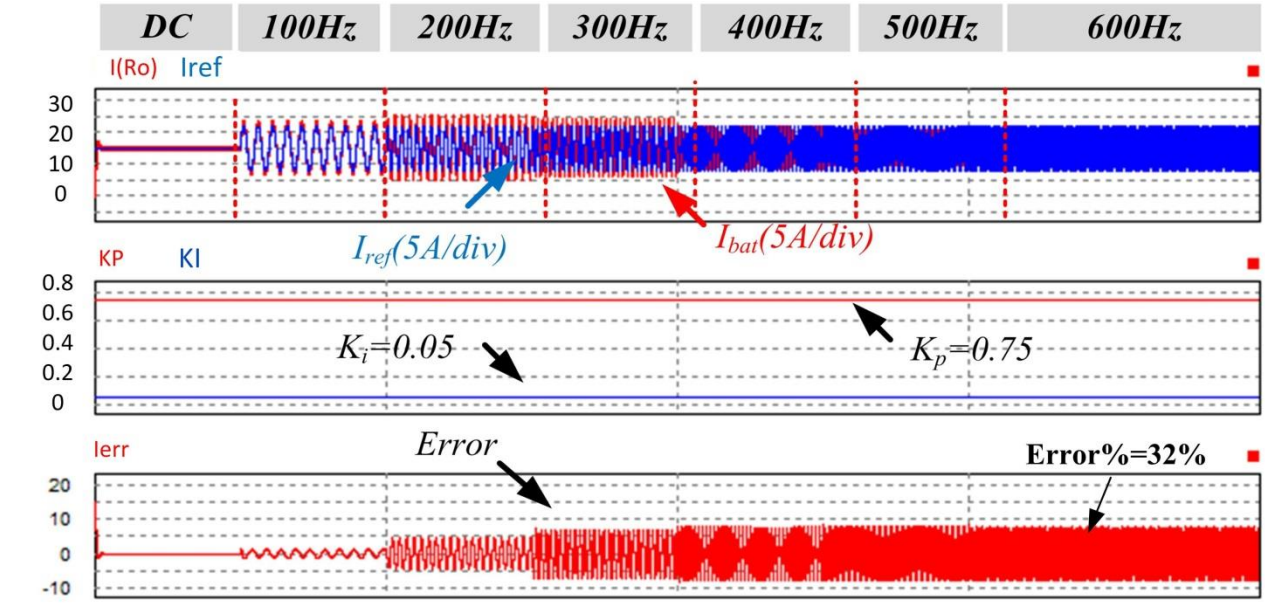

(a)

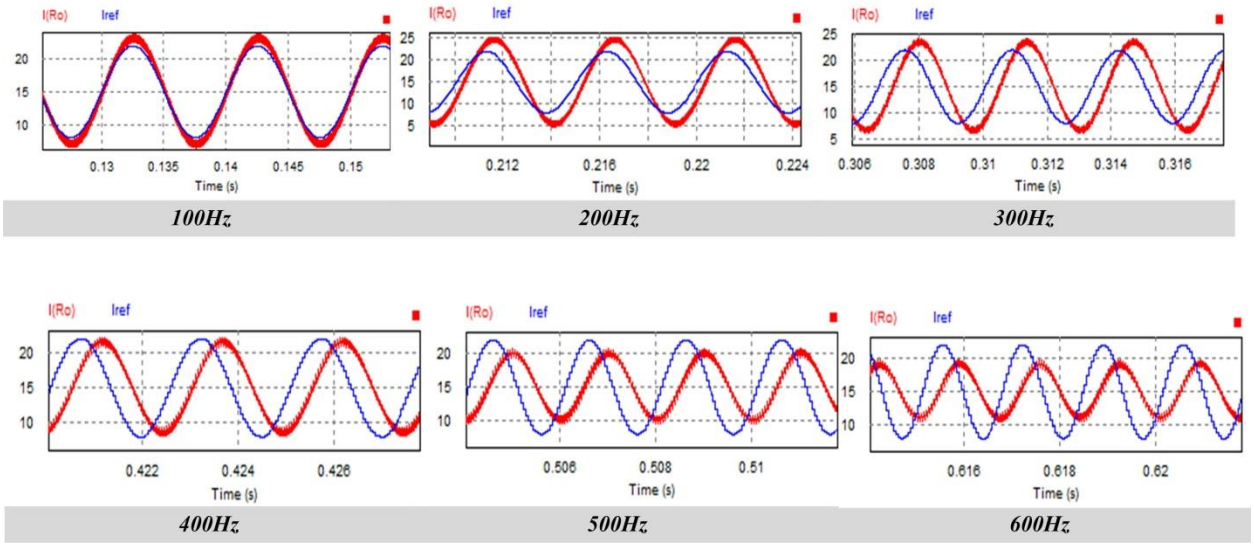

(b)

Fig.5.3. Fixed gains of PI controller: low fixed gain: (a) $K_p = 0.75, K_i = 0.05$, (b) waveform from 100 Hz~600 Hz

VI. MODEL REFERENCE ADAPTIVE CONTROL FOR SRC CHARGING CONTROL

6.1 MIT rule

The MIT rule was first developed in 1960 by the researchers of Massachusetts Institute of Technology (MIT) and used to design the autopilot system for aircraft [53]. The MIT rule can be applicable to design a controller with the MRAC scheme for a system which aims to minimize the model cost function, J(θ). The cost function is defined as a function of error between the outputs of the plant, y_p and the reference model, y_m.

$$J(\theta) = \frac{1}{2}e^2, \; e = y_p - y_m \tag{9}$$

The controller parameter, θ, is adjusted in such a fashion so that the cost function can be minimized to zero. To make cost function small, it is reasonable to change the parameters in the direction of negative gradient of J.

$$\frac{d\theta}{dt} = -\gamma \frac{\partial J}{\partial \theta} = -\gamma e \frac{\partial e}{\partial \theta} \tag{10}$$

The partial derivative term, $\partial e/\partial \theta$, is the sensitivity derivative of the error with respect to θ, which tells the error is dependent on the controller parameter θ. The γ indicates the adaptation gain of the controller.

6.2 Design of MRAC

In order to build the adaptive PI gain control, MRAC is used. The basic principle of MRAC is to build a reference model that specifies the desired output of the controller and then the adaptation algorithm adjusts the parameters of the controller so that the tracking error converges

to zero. The block diagram of the MRAC system with synchronous buck charger is shown in Fig.6.1. The system consists of two loops, an outer loop or normal feedback loop and an inner loop or parameter adjustment loop. The adaptive algorithm changes the controller parameters.

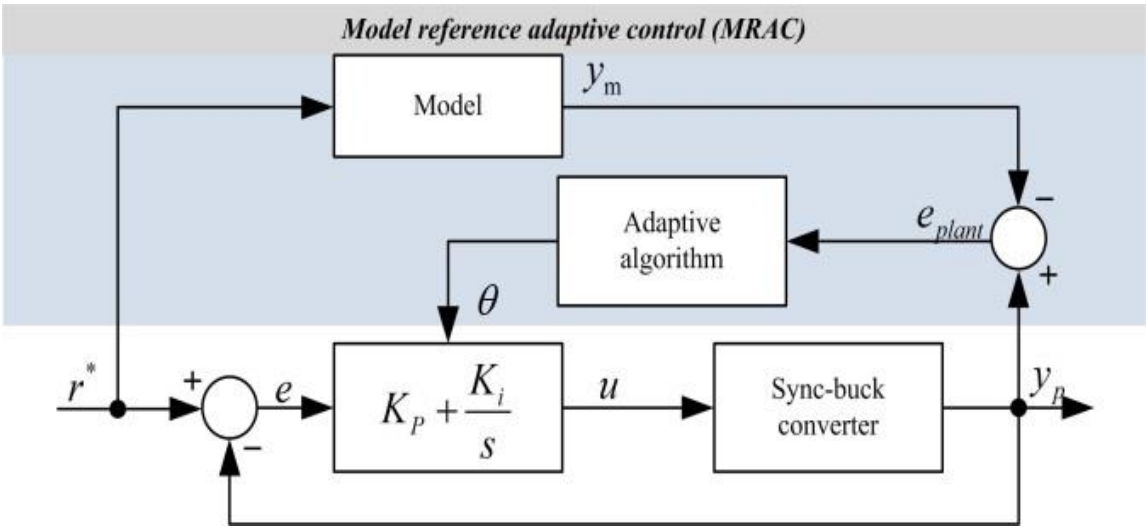

Fig.6.1. Control block diagram for integrating MRAC into the plant model

6.2.1 Design of PI controller using MRAC

The MRAC scheme is applied to adaptive PI gain controller for SRC method. In order to regulate the output current with respect to the variable frequency reference, the proposed method can adjust control gains corresponding to system parameter changes. The plant transfer function in the s-domain is as follows:

$$G(s) = \frac{b_1 s^2 + b_2 s + b_3 s}{a_1 s^2 + a_2 s + a_3} = \frac{y(s)}{u_c(s)} \tag{11}$$

where u_c is the input signal.

The input reference is an ac signal with dc offset which can be represented as follows:

$$u_c = M * \frac{w}{s^2 + w^2} + \frac{C}{s} \tag{12}$$

where M is the amplitude of sinusoidal signal, and C is the constant value of dc offset.

After introducing a PI controller, the closed-loop transfer function is obtained in (15). The MIT rule can be applied to obtain the control parameters. θ is equivalent to k_p and k_i parameters. The control parameters, k_p and k_i will be in (13-14), where $e = y_p - y_m$, then $\frac{\partial e}{\partial y} = 1, \frac{\partial J}{\partial e} = e$. Thus, we have to find $\partial y/\partial k_p$ and $\partial y/\partial k_i$ by using (15).

Taking the partial derivative of (15) with respect to k_p results in (16-17). After rearranging (18), we can obtain (19). Similarly differentiating (15) with respect to ki yields (20). In order to obtain the relationship that the controller parameters k_p and k_i are dependent upon the adaptation gain, error and the reference plant model, we substitute (19) in (13) and (20) in (14) will yield (21) and (22), respectively. These equations show the control law for adjusting the parameters kp and ki with respect to γ. The value of optimal adaptation gain was determined by manual tuning.

$$\frac{dkp}{dt} = -\gamma_{kp}\left(\frac{\partial J}{\partial kp}\right) = -\gamma_{kp}\left(\frac{\partial J}{e}\right)\left(\frac{\partial e}{\partial y}\right)\left(\frac{\partial y}{\partial kp}\right) = -\gamma_{kp}\left(\frac{\partial y}{\partial kp}\right) \tag{13}$$

$$\frac{dki}{dt} = -\gamma_{ki}\left(\frac{\partial J}{\partial ki}\right) = -\gamma_{ki}\left(\frac{\partial J}{e}\right)\left(\frac{\partial e}{\partial y}\right)\left(\frac{\partial y}{\partial ki}\right) = -\gamma_{ki}\left(\frac{\partial y}{\partial ki}\right) \tag{14}$$

$$\frac{y(s)}{u_c(s)} = \frac{b_1k_ps^3+(b_1k_i+b_2k_p)s^2+(b_2k_i+b_3k_p)s+b_3k_i}{(1+b_1k_p)s^3+(a_1+b_1k_i+b_2k_p)s^2+(a_2+b_2k_i+b_3k_p)s+b_3k_i} \tag{15}$$

$$y[(1+b_1k_p)s^3+(a_1+b_1k_i+b_2k_p)s^2+(a_2+b_2k_i+b_3k_p)s+b_3k_i]$$

$$= u_c[b_1k_ps^3+(b_1k_i+b_2k_p)s^2+(b_2k_i+b_3k_p)s+b_3k_i] \tag{16}$$

$$y\frac{\partial}{\partial k_p}\left[\left(1+b_1k_p\right)s^3+\left(a_1+b_1k_i+b_2k_p\right)s^2+\left(a_2+b_2k_i+b_3k_p\right)s+b_3k_i\right]$$

$$+\frac{\partial y}{\partial k_p}\left[\left(b_1k_p\right)s^3+\left(a_1+b_1k_i+b_2k_p\right)s^2+\left(a_2+b_2k_i+b_3k_p\right)s+b_3k_i\right]$$

$$=\frac{\partial}{\partial k_p}\left[\left(b_1k_p\right)s^3+\left(b_1k_i+b_2k_p\right)s^2+\left(b_2k_i+b_3k_p\right)s+b_3k_i\right]u_c \quad (17)$$

$$y(b_1s^3+b_2s^2+b_3s)+\frac{\partial y}{\partial k_p}[\left(1+b_1k_p\right)s^3+\left(a_1+b_1k_i+b_2k_p\right)s^2$$

$$+\left(a_2+b_2k_i+b_3k_p\right)s+b_3k_i]=u_c(b_1s^3+b_2s^2+b_3s) \quad (18)$$

$$\frac{\partial y}{\partial k_p}=\frac{(b_1s^3+b_2s^2+b_3s)}{[(1+b_1k_p)s^3+(a_1+b_1k_i+b_2k_p)s^2+(a_2+b_2k_i+b_3k_p)s+b_3k_i]}\ (u_c-y) \quad (19)$$

$$\frac{\partial y}{\partial k_i}=\frac{b_1s^2+b_2s+b_3}{[(1+b_1k_p)s^3+(a_1+b_1k_i+b_2k_p)s^2+(a_2+b_2k_i+b_3k_p)s+b_3k_i]}\ (u_c-y) \quad (20)$$

$$\frac{dk_p}{dt}=-r_p*e*\frac{(b_1s^3+b_2s^2+b_3s)}{[(1+b_1k_p)s^3+(a_1+b_1k_i+b_2k_p)s^2+(a_2+b_2k_i+b_3k_p)s+b_3k_i]}\ (u_c-y) \quad (21)$$

$$\frac{dk_i}{dt}=-r_i*e*\frac{b_1s^2+b_2s+b_3}{[(1+b_1k_p)s^3+(a_1+b_1k_i+b_2k_p)s^2+(a_2+b_2k_i+b_3k_p)s+b_3k_i]}\ (u_c-y) \quad (22)$$

The reference model can be created by a reference sine waveform with dc offset and the open loop gain model LG(s) as follows:

$$y_m(s)=(M*\frac{w}{s^2+w^2}+C*\frac{1}{s})LG(s) \quad (23)$$

Where M refers to the amplitude of the sine wave, C refers to the amplitude of dc offset of the charging current and w indicates the frequency of the reference SRC.

In the proposed model, we apply the MRAC algorithm with digital control. The control block diagram is shown in Fig.6.2.

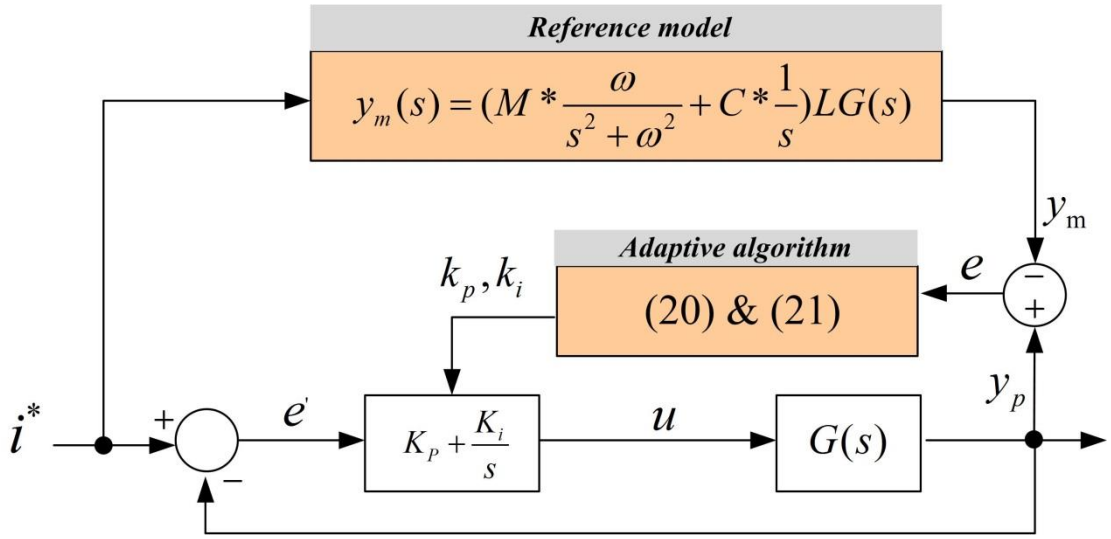

Fig.6.2. Control block diagram of the proposed method

The sinusoidal current is not only fed into the regular PI control loop, but also provided as the input to the reference model. The outputs of the plant model are expected to imitate the behavior of the reference model. The following shows the procedure of the control block diagram for integrating MRAC into the plant model.

(1) The error, e is obtained from the difference between the reference model and the plant model.

(2) After the error value get tuned by the adaptive algorithm (21) and (22), the adaptive PI gain, k_p and k_i are used to adjust the PI controller so that the closed loop dynamics of y_p is able to mirror those of a reference model.

(3) As a result, the plant model is able to achieve the desired dynamics by tracking the reference model until the error converges to zero.

6.3 Simulation

In order to obtain the optimal performance under the variable frequency input, the MRAC controller is applied to this system. As a result, the SRC is well regulated under all conditions shown in Fig.6.3 (a). The k_p and k_i gains are adjusted followed by the swept frequency and as a result, the error value is minimized shown in Fig.6.3 (a). From the simulation results, we can observe that the conventional PI gains design is for dc or low frequency condition. However, in order to apply the SRC charging method, the higher frequency input case has to be considered. In the fixed PI gain condition, the P gain dominates the response and the tracking ability; which means when the k_p gain is high; the system has high control bandwidth or faster response to track the reference current. The k_i gain affects the attenuation of the output current; when the k_i gain is high, the amplitude of output current is attenuated. In addition, we can observe in both low gain and high gain cases that even the output current is able to be regulated at low frequency range. The error increases at high frequency range because the fixed gain PI controller has no capability to handle the high frequency ripple current reference under the limitation of the system. The adaptive current controller based on MRAC shows the good tracking ability under both low frequency and high frequency range shown in Fig.6.3 (b). In addition, the error percentage is only 2.8% which is acceptable and the performance of the actual plant is approaching the performance of the reference model.

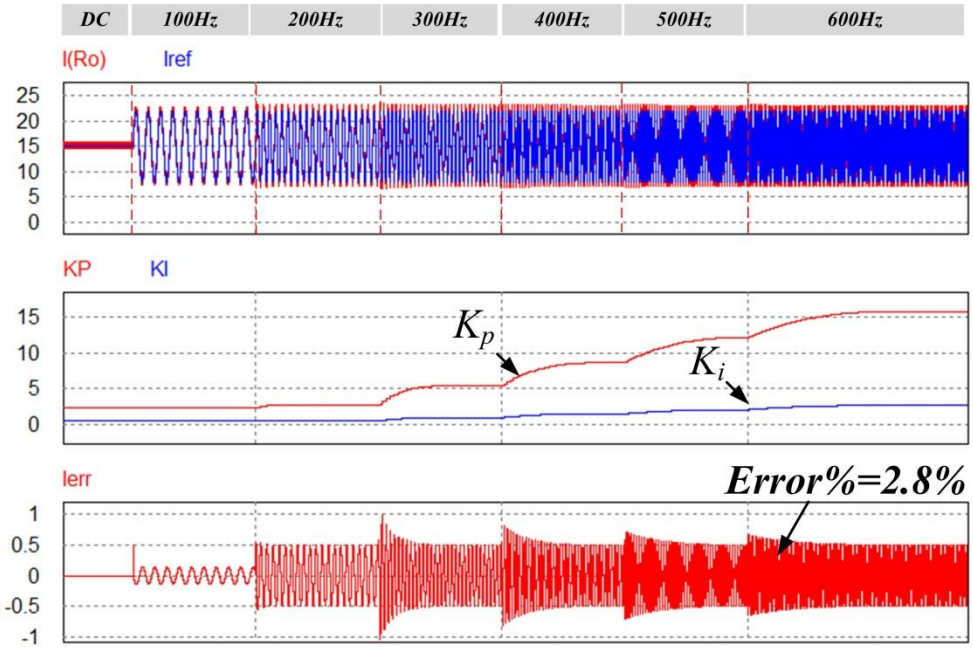

(a)

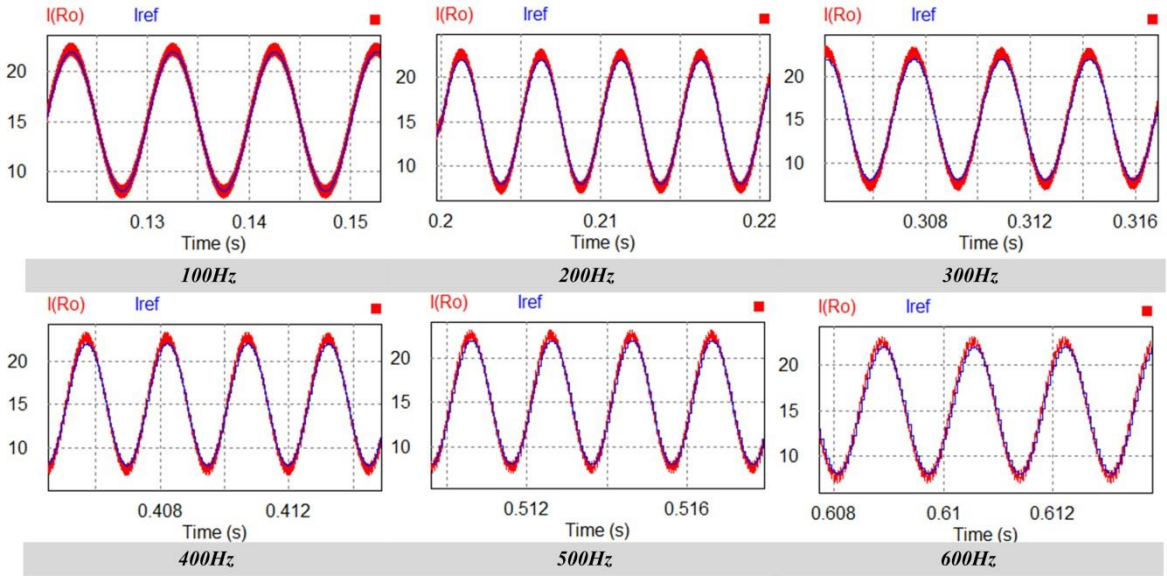

(b)

Fig.6.3. Simulation results of adaptive PI gain: (a) the overall waveforms, K_p variations, K_i variations, and error variations, (b) zoomed in few cycle waveforms with 100 ~ 600 Hz

6.4 Implemented Hardware Prototype

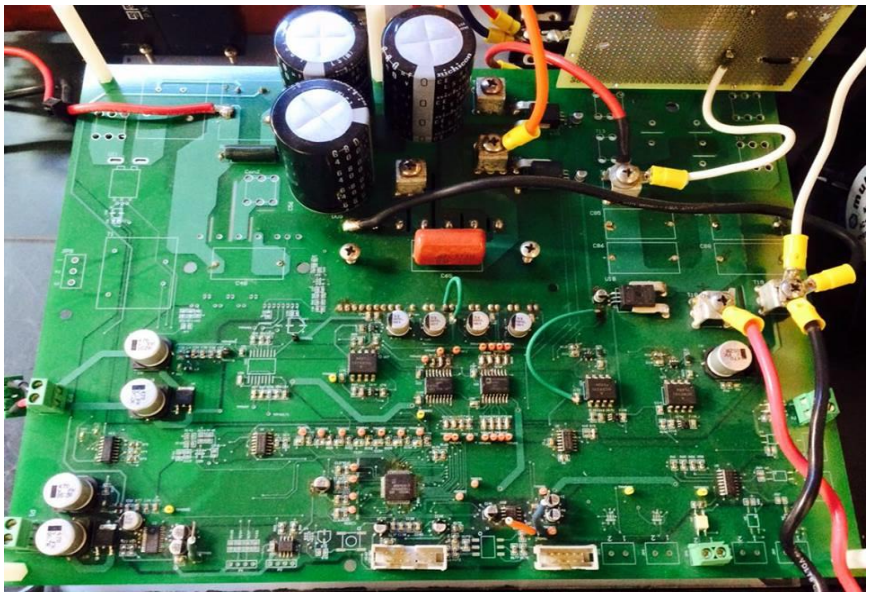

Fig.6.4. Implemented hardware prototype-synchronous buck charger system

6.5 Experimental Results

In order to verify the proposed method, the battery test is performed. In section A below, the attenuation ratios with respect to the frequency of sinusoidal ripple current are measured. Subsequently, in section B, the proposed method demonstrates the variable PI gain controller based on MRAC.

A. Attenuation with respect to ripple current frequency

Fig.6.5 shows the attenuation of ripple current with respect to the frequency. We could tell that the ripple current is well regulated at low frequency range; however, by increasing the frequency, the magnitude of ripple current is attenuated.

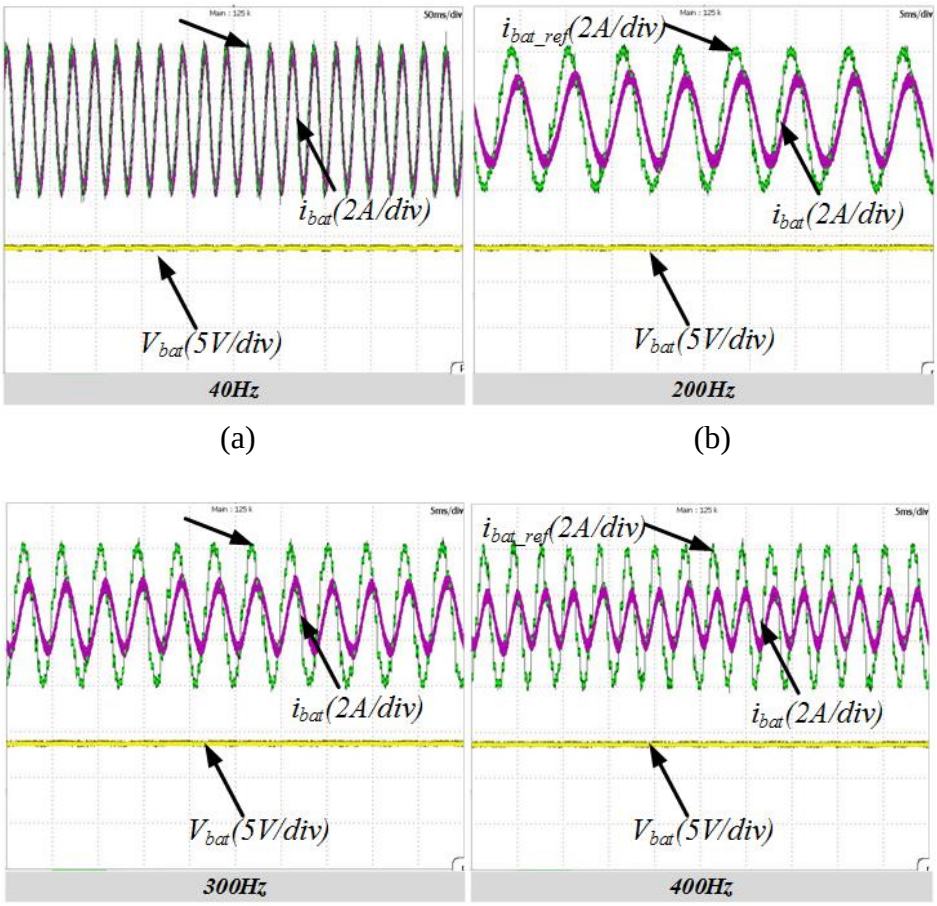

(a) (b)

(c) (d)

Fig.6.5. Attenuation of ripple current with respect to the frequency:
(a) 40Hz, (b) 200Hz, (c) 300 and (d) 400Hz.

B. Proposed adaptive PI gain based on MRAC

Fig.6.6 shows the proposed method. Before turning on the MRAC control, the magnitude of ripple current is attenuated. After turning on the MRAC control, the ripple current is well regulated. In order to verify the performance in low and high frequency, at 50 Hz and 400 Hz, the tests are performed. Both cases are well regulated.

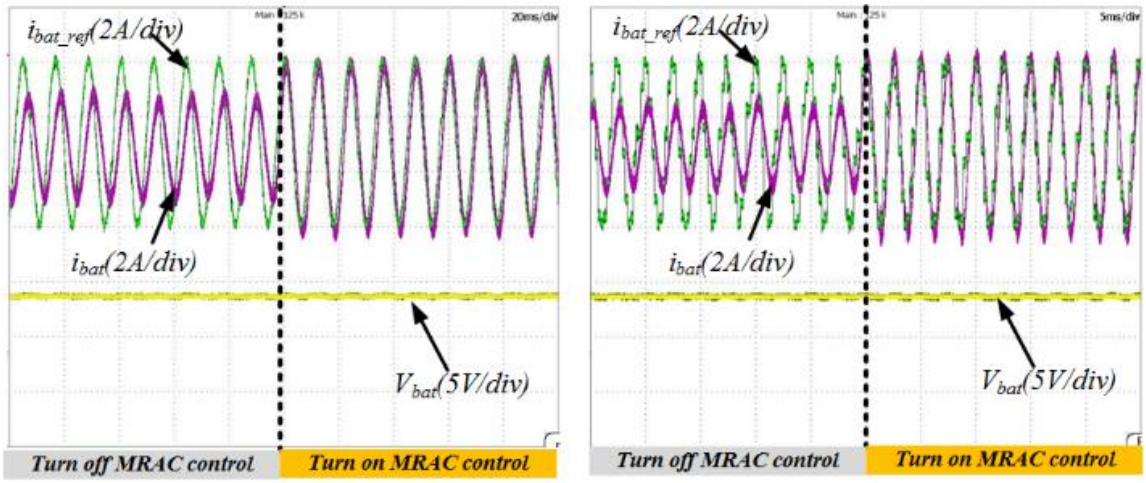

(a) (b)

Fig.6.6. Proposed control: (a) 50 Hz and (b) 400 Hz.

VII. CONCLUSIONS AND FUTURE WORK

7.1 Conclusions

The existing CCCV synchronous buck converter charging systems is analyzed followed by applying one of adaptive control method to achieve SRC have been discussed. Since existing CCCV charger systems are designed for constant current charging, the cut-off frequency and the control bandwidth limited the performance of the variable frequency ripple current control. Thus, the fixed PI gain controller is not effective in SRC charging method. In order to show the limitation of the fixed gain control, the plant model, control design, and loop gain analysis were carried out in the frequency domain. And the optimal range of cut-off frequency is found based on the perspective of the crossover frequency and the switching frequency. Simulation and experimental results clearly show the fixed gain control cannot regulate the ripple current at high frequency condition. However, the error percentage between the output of the actual plant model and the reference plant model is greatly improved with adaptive PI gain control. In addition, there is no attenuation and phase delay under the variable frequency conditions.

As a result, SRC charging method was achievable due to the correct regulation of ripple current over a wide range of frequencies with the proposed method.

7.2 Future Work

The results were obtained by manual tuning. However, the system may become poor or even unstable without defining the range of the adaptation gain, γ. Therefore, it is necessary to further investigate the analysis of stability and find out the range of the adaptation gain.

References

[1] Joe Buxton, “Designer’s Guide to Charging Li-Ion Batteries ”, Analog Devices.

[2] Walt Kester, Joe Buxton, “Battery Chargers”

[3] Henry J. Zhang, “Basic concepts of Linear Regulator and Switching mode power supplies”, Application Note, Linear Technology, October 2013

[4] Warren Schroeder, “Direct Battery Connection Benefits Portable Designs”, SEMTECH, Power Electronics Technology in July 2007

[5] Terry L. Cleveland, “Bi-directional Power System for Laptop Computers”, Microchip Technology Inc

[6] L. Huber, and M. Jovanovic, “Evaluation of flyback topologies for notebook ac-dc adapter/charger applications”, High Frequency Power Conversion Conf. Proc., May 1995, pp. 284-294

[7] M. Zhang, M. Jovanovic, and F. C. Lee, “Design considerations and performance evaluation of synchronous rectification efficiency in flyback converters,” IEEE Applied Power Electronics Conf. Proc., Feb. 1997, pp. 623-630

[8] Agilent, “Compliance Testing to the IEC 1000-3-2 (EN 61000-3-3) and IEC 1000-3-3 (EN 61000-3-3) standards”, Application Note AN 1273

[9] Garcia, O.; Cobos, J.A.; Prieto, R.; Alou, P.; Uceda, J., "Simple AC/DC converters to meet IEC 1000-3-2," Applied Power Electronics Conference and Exposition, 2000. APEC 2000. Fifteenth Annual IEEE , vol.1, no., pp.487,493 vol.1, 2000

[10] “International Energy Outlook 2009,” Energy Information Administration Office of Integrated Analysis and Forecasting U.S. Derpartment of Energy Washington DC, May 2009

[11] Texas Instruments, “Hybrid and Electric Vehicle Solutions Guide”

[12] L. Siguang, Z. Chengning, and X. Shaobo, “Research on Fast Charge Method for “Lead-acid Electric Vehicle Batteries”, in Proc. IEEE ISA’09, May 2009, pp. 1-5

[13] M.C. Kisacikoglu, B. Ozpineci, L.M. Tolbert, “Reactive power operation analysis of
a single-phase EV/PHEV bidirectional battery charger,” Power Electronics and
ECCE Asia (ICPE & ECCE), 2011 IEEE 8th International Conference on , vol., no., pp.585-592, May 30 2011-June 3 2011

[14] Donoghue, J.; Cruden, A.J., "Whole system modelling of V2G power network control, communications and management," in Electric Vehicle Symposium and Exhibition (EVS27), 2013 World , vol., no., pp.1-9, 17-20 Nov. 2013

[15] G. Joos, M. de Freige, M. Dubois, “Design and Simulation of a Fast Charging Station for PHEV/EV Batteries” Electric Power and Energy Conference (EPEC), 2010 IEEE, EPEC.2010, pp. 1 – 5, 2010

[16] Dickerman, L.; Harrison, J., "A New Car, a New Grid," in Power and Energy Magazine, IEEE , vol.8, no.2, pp.55-61, March-April 2010

[17] Yilmaz, M.; Krein, P.T., "Review of Battery Charger Topologies, Charging Power Levels, and Infrastructure for Plug-In Electric and Hybrid Vehicles," in Power Electronics, IEEE Transactions on , vol.28, no.5, pp.2151-2169, May 2013

[18] Sudipta Chakraborty, Marcelo G. Simoes, Willian E. Kramer, “Power Electronics for Renewable and Distributed Energy Systems: A sourcebook of Topologies, Control and Integration”

[19] [Online] Available: http://batteryuniversity.com/learn/article/is_lithium_ion_the_ideal_battery

[20] Cope, R.C.; Podrazhansky, Y., "The art of battery charging," Battery Conference on Applications and Advances, 1999. The Fourteenth Annual , vol., no., pp.233,235, 1999
[21] Texas Instruments “Simple CC/CV charger using TPS54331”, Application Note, SLVA551-December 2012
[22] Jingyu Yan, Guoqing Xu, Huihuan Qian, Yangsheng Xu and Zhibin Song, Energies 2011, 4(8), 1178-1196
[23] Ullah, Z.; Burford, B.; Dillip, S., "Fast intelligent battery charging: neural-fuzzy approach," Aerospace and Electronic Systems Magazine, IEEE , vol.11, no.6, pp.26,34, Jun 1996
[24] Surmann, H., "Genetic optimization of a fuzzy system for charging batteries," Industrial Electronics, IEEE Transactions on , vol.43, no.5, pp.541,548, Oct 1996
[25] Jingyu Yan, Guoqing Xu, Huihuan Qian, Yangsheng Xu and Zhibin Song, Energies 2011, 4(8), 1178-1196
[26] Yi-Hwa Liu; Yi-Feng Luo, "Search for an Optimal Rapid-Charging Pattern for Li-Ion Batteries Using the Taguchi Approach," Industrial Electronics, IEEE Transactions on , vol.57, no.12, pp.3963,3971, Dec. 2010
[27] Liang-Rui Chen, "Design of Duty-Varied Voltage Pulse Charger for Improving Li-Ion Battery-Charging Response," Industrial Electronics, IEEE Transactions on , vol.56, no.2, pp.480,487, Feb. 2009
[28] Liang-Rui Chen; Shing-Lih Wu; Deng-Tswen Shieh; Tsair-Rong Chen, "Sinusoidal-Ripple-Current Charging Strategy and Optimal Charging Frequency Study for Li-Ion Batteries," Industrial Electronics, IEEE Transactions on , vol.60, no.1, pp.88,97, Jan. 2013
[29] Liang-Rui Chen, "Design of Duty-Varied Voltage Pulse Charger for Improving Li-Ion Battery-Charging Response," Industrial Electronics, IEEE Transactions on , vol.56, no.2, pp.480,487, Feb. 2009
[30] Liang-Rui Chen; Shing-Lih Wu; Deng-Tswen Shieh; Tsair-Rong Chen, "Sinusoidal-Ripple-Current Charging Strategy and Optimal Charging Frequency Study for Li-Ion Batteries," Industrial Electronics, IEEE Transactions on , vol.60, no.1, pp.88,97, Jan. 2013
[31] Texas Instruments “Simple CC/CV charger using TPS54331”, Application Note, SLVA551-December 2012
[32] Fairchild Semiconductor, “Design Considerations for Battery Charger Using Green Mode Fairchild Power Switch”, Application Note AN4138
[33] Collin, A.J.; Djokic, S.Z.; Thomas, H.F.; Meyer, J., "Modelling of electric vehicle chargers for power system analysis," Electrical Power Quality and Utilisation (EPQU), 2011 11th International Conference on , vol., no., pp.1,6, 17-19 Oct. 2011
[34] Moaveni, B.; Abdollahzadeh, H.; Mazoochi, M., "Adjustable output voltage Zeta converter using neural network adaptive model reference control," Control, Instrumentation and Automation (ICCIA), 2011 2nd International Conference on , vol., no., pp.552,557, 27-29 Dec. 2011
[35] Chan, C.C.; Chau, K.T., "An overview of power electronics in electric vehicles," in Industrial Electronics, IEEE Transactions on , vol.44, no.1, pp.3-13, Feb 1997
[36] Mehdi Javdani Erfani, “Design of a Bidirectional On-board Battery Charger in Hybrid Electric Vehicle Applications”, Chalmers University of Technology, 2011
[37] [Online available] http://www.nytimes.com/2008/11/20/automobiles/autoshow/mini-e.html?_r=0
[38] [Online available] https://en.wikipedia.org/wiki/Tesla_Roadster
[39] L. Tang and G.-J. Su, “A low-cost, digitally-controlled charger for plug-in hybrid electric vehicles," in IEEE Energy Conversion Congr. Expo. (ECCE), San Jose, CA, Sep. 20, 2009

[40] Clarke, D.W., "Pretuning and adaptation of PI controllers," Control Theory and applications, IEE Proceedings - , vol.150, no.6, pp.585,598, 21 Nov. 2003
[41] Yasser, M.; Trisanto, A.; Jianming Lu; Sekiya, H.; Yahagi, T., "Adaptive sliding mode control using simple adaptive control for SISO nonlinear systems," in Circuits and Systems, 2006
[42] Priyank Jain and M.J. Nigam, "Design of a Model Reference Adaptive Controller Using Modified MIT Rule for a Second Order System", Advance in Electric and Electric Engineering ISSN 2231-1297
[43] Yong-Duk Lee; Sung-Yeul Park; Soo-Bin Han, "Online Embedded Impedance Measurement Using High-Power Battery Charger," in Industry Applications, IEEE Transactions on , vol.51, no.1, pp.498-508, Jan.-Feb. 2015
[44] Rich Nowakowski and Ning Tang, "Efficiency of synchronous versus nonsynchronous buck converters", Texas Instruments, 2009
[45] "Power Inductors 8 Design Tips", WURTH ELEKTRONIK
[46] Lloyd Dixon, "Control Loop Design", Texas Instrument, 2001
[47] Siri, K., "Study of system instability in current-mode converter power systems operating in solar array voltage regulation mode," in Applied Power Electronics Conference and Exposition, 2000. APEC 2000. Fifteenth Annual IEEE , vol.1, no., pp.228-234 vol.1, 2000
[48] Hae-Gwang Jeong; Kyo-Beum Lee, "A controller design of quick chargers with a current offset compensator," in Vehicle Power and Propulsion Conference (VPPC), 2012 IEEE , vol., no., pp.695-699, 9-12 Oct. 2012
[49] Robert W. Erickson, Dragan Maksimovic, "Fundamental of Power Electronics",1997-2004
[50] Hank Zumbahlen, "Fo and Q in filters", Analog Devices, 2012
[49] Lee, Y.; Park, S., "Electrochemical State-Based Sinusoidal Ripple Current Charging Control," Power Electronics, IEEE Transactions on , vol.30, no.8, pp.4232,4243, Aug. 2015
[51] Ridley, R.B., "Secondary LC filter analysis and design techniques for current-mode-controlled converters," Power Electronics, IEEE Transactions on , vol.3, no.4, pp.499,507, Oct 1988
[52] [Online available] https://www.valence.com/products/standard-modules/xp-module/
[53] Priyank Jain; Dr. M.J. Nigam ., "Design of a Model Reference Adaptive Controller Using Modified MIT Rule for a Second Order System," Advance in Electronic and Electric Engineering, ISSN 2231-1297, Volume 3, Number 4 (2013)

Appendix A: Simulation in PSIM

The following are the simulation model of synchronous buck charger with adaptive PI control in PSIM and the coding of adaptive PI control, respectively.

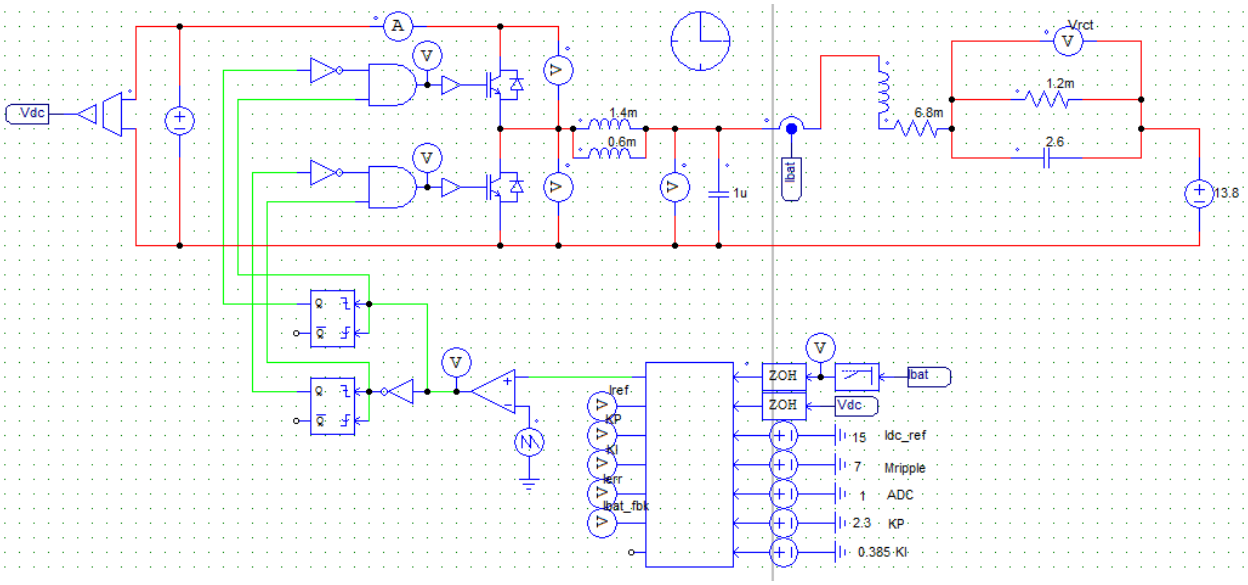

Fig.7. Simulation of synchronous buck charger model in PSIM

```
#include <Stdlib.h>
#include <String.h>
#include <math.h>
#include <Psim.h>


#define     TwoPI      6.283
// PLACE GLOBAL VARIABLES OR USER FUNCTIONS HERE...

static double     Ibat_fbk=0,      Vdc=0,Inv_Vdc =0;
static double     Iref_dc=0,Iref_ac=0;
static double     Ierr=0,VP=0,VINT=0,      VF=0,Vreal=0;
static double     Vbat_Limit=0;
static double     Duty=0;
static double     KP=15, KI=0.2;
static double     KP_P=0,KP_I=0,KI_P=0,KI_I=0;

static double     D_Angle=0,PLL=0, Angle1=0, Sin_Angle=0;
```

```
static double     Fs=0;

static int   ADC=0,ADControl=0;;

//////////////////////////////////////////////////////////////////////
// FUNCTION: SimulationStep
//      This function runs at every time step.
//double t: (read only) time
//double delt: (read only) time step as in Simulation control
//double *in: (read only) zero based array of input values. in[0] is the first node, in[1] second input...
//double *out: (write only) zero based array of output values. out[0] is the first node, out[1] second output...
//int *pnError: (write only)    assign    *pnError = 1;    if there is an error and set the error message in szErrorMsg
//       strcpy(szErrorMsg, "Error message here...");
void SimulationStep(
            double t, double delt, double *in, double *out,
              int *pnError, char * szErrorMsg,
              void ** reserved_UserData, int reserved_ThreadIndex, void * reserved_AppPtr)
{
      Ibat_fbk   = in[0];
      Vdc                  = in[1];
      Inv_Vdc        = 1/Vdc;
      Iref_dc             = in[2];
      Iref_ac             = in[3];
      ADControl = in[4];

      Ierr =    (Iref_dc+Iref_ac*Sin_Angle) - Ibat_fbk;

      if((ADControl == 1) && Ierr >0.5){
//    if( ADControl == 1 ){
            KP_P =Ierr*0.05;    //0.2
            KP_I    +=Ierr*0.03;    //0.15
            KP = KP_P+KP_I;

            KI_P =Ierr*0.005;    //0.02
            KI_I    +=Ierr*0.005;    //0.02
            KI = KI_P+KI_I;

      }
      else if(ADControl == 0){
            KP = in[5];
            KI    = in[6];
```

```
    }



    VP   = KP*Ierr;
    VINT +=KI*Ierr;

    VF = VP+VINT;
    Vbat_Limit = Vdc*0.9;
    Vreal = ((VF> Vbat_Limit) ?    Vbat_Limit : (VF< 0) ? 0: VF);

    Duty = Vreal*Inv_Vdc;

    out[0]      = Duty;
    out[1]      = Iref_dc+Iref_ac*Sin_Angle;
    out[2]      = KP;
    out[3]      = KI;
    out[4]      = Ierr;
    out[5]      = Ibat_fbk;


    if(ADC==2000){
        ADC = 0;
        if(Fs == 600) Fs = 600;
        else Fs +=100;
    }

    D_Angle = 2*3.14*50e-6*Fs;
    PLL                 = Angle1+D_Angle;
    if(PLL > 3.14)                  Angle1    = PLL-TwoPI;
    else if (PLL <-3.14)  Angle1    = PLL+TwoPI;
    else                                Angle1    = PLL;
    Sin_Angle=sin(Angle1);

    ADC++;

}
```

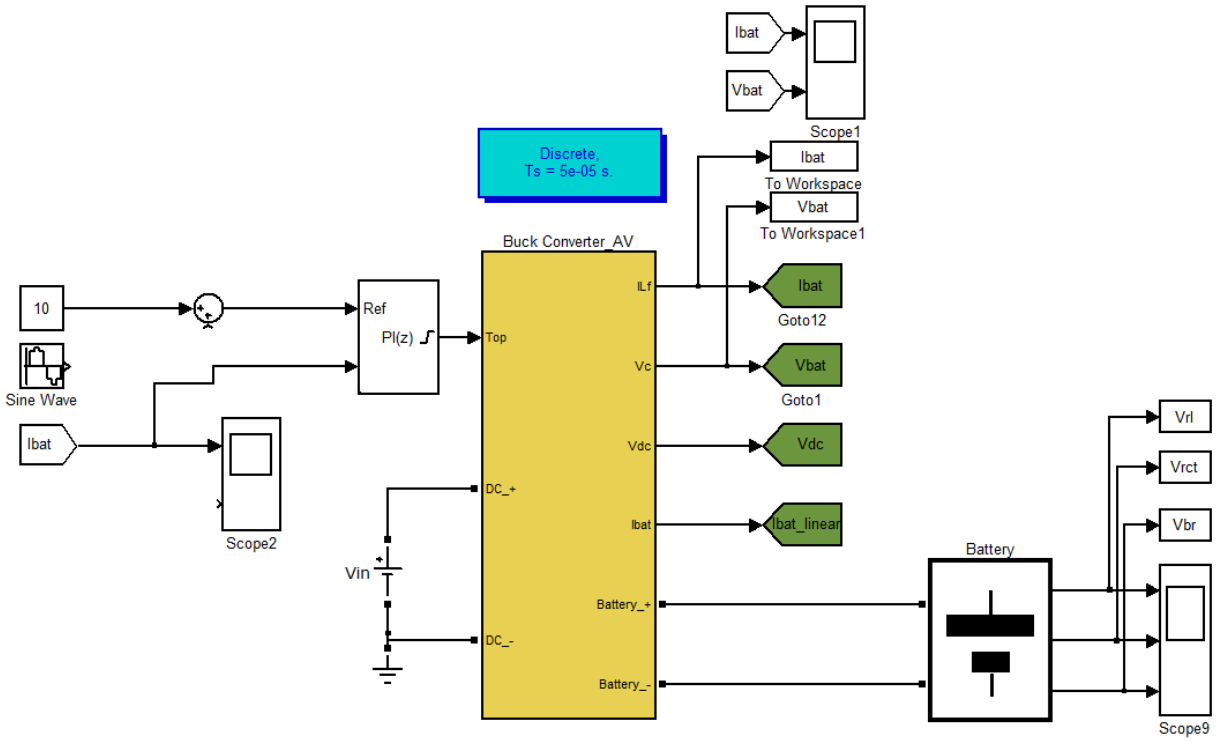

Fig.8. (a) Simulation of synchronous buck charger model in Simulink

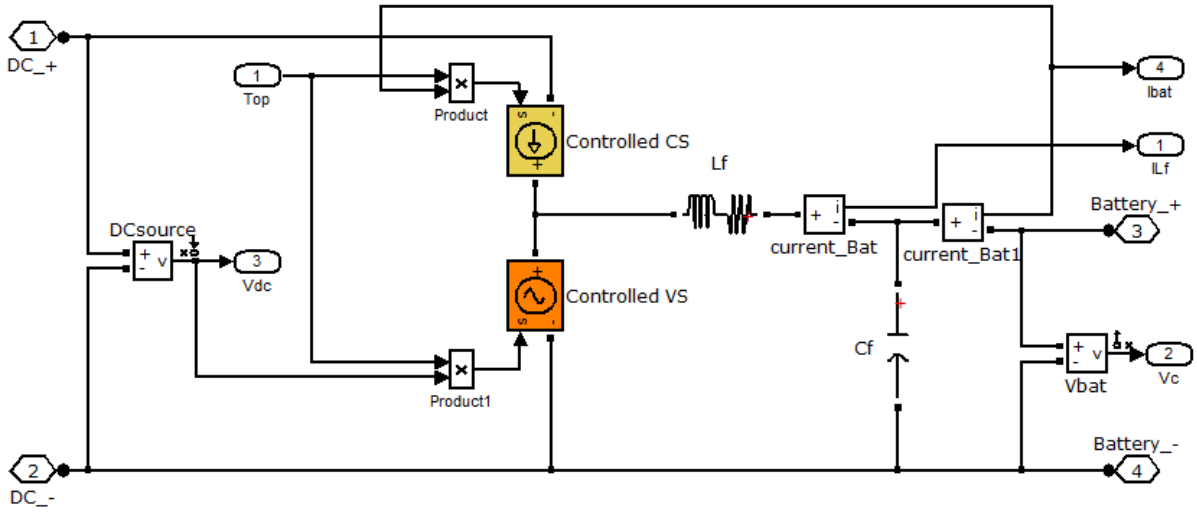

Fig.8. (b) Topology of synchronous buck charger model

Appendix C: Publications

[1]. Jen-Guey Chen; Yong-Duk Lee; Sung-Yeul Park, "Adaptive PI gain control to realize sinusoidal ripple current charging," in *Power Electronics and ECCE Asia (ICPE-ECCE Asia), 2015 9th International Conference on* , vol., no., pp.2582-2589, 1-5 June 2015